Resource Allocation for Power Minimization in RIS-assisted Multi-UAV Networks with NOMA

Wanmei Feng, *Member, IEEE*, Jie Tang, *Senior Member, IEEE*, Qingqing Wu, *Senior Member, IEEE*, Yuli Fu, Xiuyin Zhang, *Fellow, IEEE*, Daniel K. C. So, *Senior Member, IEEE* and Kai-Kit Wong, *Fellow, IEEE*

***Abstract*—Reconfigurable intelligent surface (RIS) is a promising technique that smartly reshapes wireless propagation environment in the future wireless networks. In this paper, we apply RIS to an unmanned aerial vehicle (UAV)-assisted non-orthogonal multiple access (NOMA) network, in which the transmit signals from multiple UAVs to ground users are strengthened through RIS. Our objective is to minimize the power consumption of the system while meeting the constraints of minimum data rate for users and minimum inter-UAV distance. The formulated optimization problem is non-convex by jointly optimizing the position of UAVs, RIS reflection coefficients, transmit power, active beamforming vectors and decoding order, and thus is quite hard to solve optimally. To tackle this problem, we divide the resultant optimization problem into four independent subproblems, and solve them in an iterative manner. In particular, we first consider the sub-solution of UAVs placement which can be obtained via the successive convex approximation (SCA) and maximum ratio transmission (MRT). By applying the Gaussian randomization procedure, we yield the closed-form expression for the RIS reflection coefficients. Subsequently, the transmit power is optimized using standard convex optimization methods. Finally, a dynamic-order decoding scheme is presented for optimizing the NOMA decoding order in order to guarantee fairness among users. Simulation results verify that our designed joint UAV deployment and resource allocation scheme can effectively reduce the total power consumption compared to the benchmark methods, thus verifying the advantages of combining RIS into the multi-UAV assisted NOMA networks.**

***Index Terms*—Non-orthogonal multiple access (NOMA), resource allocation, unmanned aerial vehicles (UAVs), reconfigurable intelligent surface (RIS)**

This paper has been presented in part at IEEE ICC 2022. This work has been supported in part by the National Key Research and Development Program of China under Grant 2019YFB1804100, in part by the National Natural Science Foundation of China under Grant 61971194, 62222105, 31971797, 32271997, in part by the Special Project for Guangxi Science and Technology Bases and Talents under Grant AD21075054, in part by the Open Research Fund of Guangdong Key Laboratory of Aerospace Communication and Networking Technology under Grant 2018B030322004, and in part by the International Science and Technology Cooperation Project of Guangzhou (Huangpu) under Grant 2020GH06, in part by the Science and Technology Projects of Guangzhou under Grant 202201011233, in part by the China Agriculture Research System of MOF and MARA (CARS-26). (*Corresponding author: Jie Tang*.)

W. Feng is with the College of Electronic Engineering (College of Artificial Intelligent), South China Agricultural University, Guangzhou, China. (e-mail: wmfeng@scau.edu.cn).

J. Tang, Y. Fu and X. Zhang are with the School of Electronic and Information Engineering, South China University of Technology, Guangzhou, China. (e-mail: eejtang@scut.edu.cn; fuyuli@scut.edu.cn; zhangxiuyin@scut.edu.cn).

Q. Wu is with the Department of Electronic Engineering, Shanghai Jiao Tong University, 200240, China (e-mail: qingqingwu@sjtu.edu.cn).

D. K. C. So is with the School of Electrical and Electronic Engineering, University of Manchester, Manchester, United Kingdom. (e-mail: d.so@manchester.ac.uk).

K.-K Wong is with the Department of Electronic and Electrical Engineering, University College London, London, United Kingdom. (e-mail: kai-kit.wong@ucl.ac.uk).

I. Introduction

THE dramatic proliferation of Internet-of-Things (IoT) has caused the ever-growing number of wireless devices, which are envisioned to support smart applications including automatic manufacturing, virtual reality, smart homes and smart city [1]. To this end, high performance requirements such as low-latency communication, ultra-high capacity, and massive connectivity must be met. Non-orthogonal multiple access (NOMA) is viewed as one of the emerging solutions for meeting these stringent requirements. By employing superposition coding (SC) at the transmitter side and successive interference cancellation (SIC) at the receiver side, NOMA can simultaneously serve several users with the same physical resource (i.e., time, frequency and code) [2], [3]. This makes NOMA capable of increasing the connection density and enhancing the spectral efficiency (SE). Nevertheless, despite the advantages provided by NOMA schemes, the performance gain of NOMA is still fundamentally limited by signal propagation environments, especially for users with small channel gain differences.

Recently, reconfigurable intelligent surface (RIS) is a potential technique for controlling the wireless propagation environments [4], [5]. In particular, RIS is a planar surface structure comprised of multiple low-power reflecting units, where each unit is smartly tuned by programming integrated circuits (ICs) with different amplitude and phase of the reflected signals [5], [6]. This enables the reflected signal propagations to be reconfigured, thus improving the communication quality. If NOMA and RIS are properly combined, the channel conditions of users can be changed flexibly by adjusting phase shifts at the RIS, which adds new degree-of-freedom (DoF) for improving the system performance [7]–[12]. For example, a sequential rotation scheme was presented in [7] to minimize the power consumed by a RIS-aided downlink NOMA system subject to the minimum signal-to-interference-ratio (SINR) thresholds, where the power control and RIS reflection coefficients were jointly considered. In [8], an energy minimization framework was studied in a RIS-empowered NOMA network, where the transmit beamforming and the phase shifts at the RIS were optimized, and solved by the alternating optimization approach. In [9], a three-step resource scheduling method was investigated to maximize the total throughput by considering the channel allocation, NOMA decoding order and

RIS reflection matrix in a RIS-assisted NOMA system. In [10], a resource management strategy was investigated to maximize the total throughput of a RIS-assisted uplink NOMA network subject to transmit power constraints, where the power control and RIS phase shift matrix were optimized. In [11], a weighted sum-rate maximization problem was investigated in a RIS-assisted NOMA network, in which the deployment of RIS and RIS reflection coefficients in addition to power allocation were considered, and tackled via the monotonic optimization method and semidefinite relaxation approach. In [12], an effective approach was proposed to maximize the energy efficiency (EE) in RIS-NOMA networks, where the active beamforming vectors and RIS reflection coefficients were taken into account. However, since the RISs deployed on facades of buildings or walls can only serve users distributed in the front half-space, it is difficult to meet the quality-of-service (QoS) of edge users in terrestrial RIS-enhanced wireless networks.

Due to the advantages of high mobility, autonomy and low-cost, unmanned aerial vehicles (UAVs) can be promptly dispatched to provide reliable services for edge users, and thus it has been extensively used in many fields including information dissemination [3], mobile edge computing (MEC) [13], wireless relay networks [14], wireless power transfer [15] and secure communication systems [16]. By applying RIS into UAV-assisted wireless networks, "virtual" line-of-sight (LoS) links between UAVs and ground users can be created by adjusting the phase reflection coefficients and the placement of UAVs. In particular, there are two kinds of architecture diagrams in RIS-based UAV systems. On one hand, the RISs are placed at fixed locations on the ground, which can enhance the received signal power from UAVs to edge users. The other architecture diagram is called aerial RIS (ARIS), where UAVs are equipped with a RIS to achieve intelligent control from the sky. As such, the network coverage for a given geographical area can be significantly enhanced. Consequently, RIS-based UAV communications have received much attention in the academia [17]–[24]. The authors in [17] aimed at maximizing the average achievable rate in a RIS-aided UAV system, where the UAV flight planning and RIS reflection matrix were considered. In [18], a parametric approximation approach and an iterative optimization approach were employed to maximize the system throughput in a RIS-aided UAV orthogonal frequency division multiplexing Access (OFDMA) system, in which the flight trajectory of UAV, RIS scheduling and communication resource allocation were optimized. In [19], an effective scheme was investigated to maximize the received signal strength in a multi-RIS-aided UAV network, where a closed-form solution for the RIS reflection coefficients was obtained. In [20], a RIS-assisted UAV scheme was proposed to enhance the system performance in UAV communication networks, in which closed-form solutions for the outage probability, average throughput and bit-error-rate (BER) were investigated. In [21], the problem of maximizing the minimum SINR was studied in an ARIS-enabled wireless communication system, where the transmit beamforming, 3D passive beamforming and horizontal ARIS placement were optimized. In [22], the authors investigated three different transmission schemes for a UAV-RIS relaying system, where the closed-form solutions for EE, ergodic capacity and outage probability were derived. An efficient iterative method for a RIS-assisted uplink wireless communication network was presented in [23] to maximize the secure EE, in which the trajectory of the UAV, RIS reflection matrix, user association and power allocation were considered. The authors in [24] studied the total transmit power minimization problem in UAV-assisted RIS heterogeneous networks, where the trajectory/velocity of UAVs, active beamformers, subcarrier allocations and RISs' phase shifts are jointly optimized. Simulation results demonstrated that the transmit power of the system could be significantly reduced compared with the benchmark schemes. Based on the previous researches on RIS-aided UAV communications, the application of NOMA within UAV-RIS wireless networks can further improve the SE and support massive connectivity [25], [26]. A deep-Q-network (D-DQN) based method was studied in [25] to optimize the movement of the UAV, RIS phase-shift matrix, transmit power and NOMA decoding orders, in order to minimize the total energy cost of UAV-RIS wireless networks. In [26], a sum-throughput maximization problem was investigated in a RIS-aided multi-UAV NOMA system, in which the position and power allocation of UAVs, RIS's phase-shift matrix and NOMA decoding orders were optimized, and solved by the block coordinate descent (BCD)-based method.

A. Main Contributions

Prior works concentrate on investigating the resource allocation schemes for RIS-assisted NOMA systems [7]–[12], where the UAVs are not considered to provide reliable services for edge users. On the other hand, if UAVs are applied to RIS-asssited NOMA systems, line-of-sight (LoS) transmission links between access points and edge users are established to improve system performance by adjusting its locations. Moreover, the works in [17]–[24] focus on maximizing the system performance in RIS-assisted UAV networks [17]–[20], ARIS-enabled wireless communication networks [21]–[24]. However, these algorithms do not fully exploit NOMA for improving the system throughput, especially when the users are located in ultra-dense wireless networks. In this case, these schemes may not meet the QoS requirements of massive access and cause severe interference. In addition, the work in [25] focuses on minimizing the energy cost in RIS-NOMA UAV networks. However, this scheme cannot be applied directly to design effective resource allocation policies for users distributed in specific areas since only a single UAV is taken into account. In particular, a single UAV used in specific scenarios such as disaster areas and vehicular networks, may not be able to finish complicated tasks. This leads to its limitations in large-scale applications. The work in [26] aims to investigate the resource allocation strategy for a RIS-enhanced multi-UAV NOMA network, while assuming a single antenna mounted on both UAVs and users. In this case, users will experience severe interference from other co-channel UAVs. Thus, the algorithm in [26] may not meet the QoS demands of users and reduce the energy cost of the system, particularly in users with weak channel quality. UAV equipped with multiple antennas can

separate users with angular separation, and thus mitigates co-channel interference and improve network performance [27]. Inspired by the previous observations, we investigate a RIS-assisted multi-UAV network with NOMA, where all UAVs equipped with multiple antennas establish communication links with users through the RIS. By considering the optimization of UAVs placement control, RIS reflection coefficients and resource allocation, this framework not only strengthens the signal reception at users and mitigates co-interference, but also satisfies the QoS metrics of massive access. Besides, through dynamically controlling the locations of UAVs and realizing the cooperation between UAVs and RIS, this framework provides reliable communication services to edge users, and thereby can be adopted in many applications including disaster areas, wide areas, vehicular networks and ultra-dense wireless networks. The contributions are outlined as follows.

- We formulate a NOMA-based resource allocation framework for a RIS-enabled multi-UAV system. Our objective is to minimize the total power consumption while meeting the constraints of the minimum data rate for users and a minimum inter-UAV distance. The design optimization problem is non-convex by jointly optimizing the UAV's position, RIS reflection coefficients, active beamforming vectors and decoding order, which is extremely hard to tackle directly. Therefore, we develop a joint UAV deployment and resource allocation scheme to address this issue.
- In particular, we divide the considered problem into four sub-problems, and optimize the position of UAVs, active beamforming vectors, RIS reflection matrix, transmit power and decoding order in an iterative manner. By applying maximum ratio transmission (MRT), we first yield the closed-form solution for the active beamforming vectors. Based on the solved beamforming vectors, we reformulate the power consumption minimization problem with the constraint of average minimum data rate, from which we consider the sub-solution of the UAV's position that can be achieved through the successive convex approximation (SCA) technique. Then, we derive a closed-form expression for the RIS reflection coefficients by the Gaussian randomization procedure. After that, effective convex optimization methods are applied to optimize the transmit power. Finally, we present a dynamic-order decoding scheme to optimize the NOMA decoding order.
- Simulation results show that our designed joint UAV placement and resource allocation algorithm can effectively reduce the total power consumption compared to the benchmark methods, thus verifying the advantages of combining RIS into the multi-UAV assisted NOMA networks.

B. Organization and Notation

The remainder of this paper is outlined as belows. The channel model for RIS-assisted multi-UAV systems and the sum-power minimization problem are presented in Section II. In Section III, the joint UAV placement and resource allocation scheme is presented to tackle the power minimization problem. Simulation results are presented to demonstrate the superior performance of our proposed algorithm in Section IV. Conclusions are drawn in Section V.

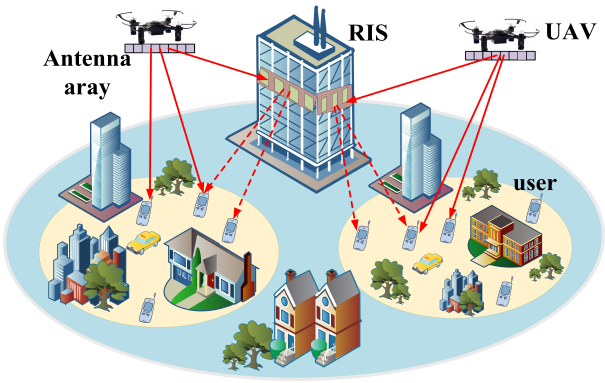

Fig. 1: Illustration of a RIS-assisted multi-UAV system with NOMA.

The notations are exploited in this paper. $\mathbf{a}^T$ and $\mathbf{a}^H$ indicate the transpose and conjugate transpose of the vector $\mathbf{a}$. $[\mathbf{a}]_m$ and $\|\mathbf{a}\|$ indicate the mth unit and the Euclidean norm of the vector $\mathbf{a}$. $\mathbb{C}^{x\times y}$ represents the space of $x \times y$ complex-value vectors. $\mathbf{A}$ denotes a matrix, and tr($\mathbf{A}$) is the trace of $\mathbf{A}$. rank($\mathbf{A}$) is the rank of $\mathbf{A}$ and $\mathbf{A}^{\frac{1}{2}}$ is the square-root of $\mathbf{A}$. $\mathbf{A} \succeq 0$ indicates that $\mathbf{A}$ is positive semi-definite. For any arbitrary-size matrix $\mathbf{S}$, $\mathbf{S}^H$ and $\mathbf{S}^T$ denote the conjugate transpose and transpose. $\mathbf{0}$ and $\mathbf{I}$ represent the all-zero matrix and the identity matrix. $\mathbb{E}\{\cdot\}$ indicates statistical expectation and Re$\{\cdot\}$ represents the real part. $\angle a$ indicates the phase of the complex number a.

II. System Model and Problem Formulation

A. System Model

As depicted in Fig. 1, we consider a RIS-assisted multi-UAV network, in which K rotary-wing UAVs are dispatched as flying base stations (BSs) providing wireless services to N_u ground users. Since the direct links between UAVs and ground users are obstructed by obstacles, a RIS with N reflecting units is placed on the ground to reflect the received signals from UAVs to users [1]. All the UAVs are setup with N_t antennas and each user has single antenna. In particular, it is assumed that the ground users are static and their locations (i.e., GPS location information) are known by UAVs. The N_u ground users is divided into K groups, wherein each group can only connect to an UAV. We denote the indices of UAVs and its corresponding connected user groups by $\mathcal{K} = \{1, 2, \cdots, K\}$ and the indices of users in the kth group by $\mathcal{M}_k = \{1, 2, \cdots, M_k\}$. Define the location of the (k, i)th user as $\mathbf{w}_i^k = [x_i^k, y_i^k, z_i^k]^T, \forall i \in \mathcal{M}_k, k \in \mathcal{K}$, while the location of the RIS is denoted as $\mathbf{w}_r = [x_r, y_r, z_r]^T$. The 3D location of the kth UAV is $\mathbf{q}_k = [x_k, y_k, H]^T$. Here, the

[1]Noted that the conventional channel estimation methods can be exploited to evaluate the UAV-RIS channel and the RIS-user channels [28]. In this paper, it is assumed that the parameters of the combined channels are estimated by the channel estimation scheme in [29]. In particular, the short-OFDM symbols through the inverse discrete Fourier transform (IDFT) are first used for channel training. Then, the least-squares (LS) estimation scheme is employed to evaluate the parameters of the direct channel and the cascaded channels. Finally, the minimum mean squared error (MMSE) is used for LS channel estimation to further diminish the computational complexity.

altitude of all UAVs are fixed at H, which corresponds to the minimum altitude required for covering serving areas and avoiding buildings. $\Theta = \text{diag}(e^{j\theta_1}, \cdots, e^{j\theta_n}, \cdots, e^{j\theta_N})$ is the RIS reflection matrix, where $\theta_n \in [0, 2\pi)$ denotes the phase shift parameter of the nth reflecting unit.

B. Channel Model for RIS-assisted multi-UAV networks

Similar to [17], [18], the links between the RIS and UAVs are assumed to be LoS-dominated since UAVs fly at high altitudes and the RIS can be properly deployed on the facade of building. Let λ and d be the wavelength and the antenna separation [30]. We denote the cosine of angle-of-arrival (AoA) and angle-of-departure (AoD) of signals as $\cos\varphi_k$ and $\cos\psi_k$, which holds $\cos\varphi_k = \cos\psi_k = \frac{x_r - x_k}{\|\mathbf{w}_r - \mathbf{q}_k\|}$ [26], [31]. The channel between the kth UAV to the RIS is [19]

$$\mathbf{g}_k = \sqrt{\frac{\rho_0}{\|\mathbf{q}_k - \mathbf{w}_r\|^2}}\bar{\mathbf{g}}_k^T \tilde{\mathbf{g}}_k, \tag{1}$$

where ρ_0 indicates the path loss at the reference distance of 1 meter. $\bar{\mathbf{g}}_k$ and $\tilde{\mathbf{g}}_k$ indicate the array responses that can be expressed as

$$\bar{\mathbf{g}}_k = [1, e^{-j\frac{2\pi d}{\lambda}\cos\varphi_k}, \cdots, e^{-j\frac{2\pi d(N-1)}{\lambda}\cos\varphi_k}]^T, \tag{2}$$

$$\tilde{\mathbf{g}}_k = [1, e^{-j\frac{2\pi d}{\lambda}\cos\psi_k}, \cdots, e^{-j\frac{2\pi d(N_t-1)}{\lambda}\cos\psi_k}]^T. \tag{3}$$

On the other hand, since there exists local scatterers around the ground nodes and the UAVs/RIS are deployed at high altitude, the channels between UAV/RIS and users include both the LoS and NLoS components [32]. Thus, we employ the Rician channel model for the UAV-user links and RIS-user links. Then, the channel between the jth UAV to the (k,i)th user is written as [18]

$$\mathbf{h}_{k,i}^j = \sqrt{\frac{\rho_0}{\|\mathbf{q}_j - \mathbf{w}_i^k\|^{\alpha_{ug}}}}\left(\sqrt{\frac{\kappa_{ug}}{\kappa_{ug}+1}}\overline{\mathbf{h}}_{k,i}^j + \sqrt{\frac{1}{\kappa_{ug}+1}}\widetilde{\mathbf{h}}_{k,i}^j\right), \tag{4}$$

where $\overline{\mathbf{h}}_{k,i}^j$ indicates the deterministic LoS component, $\widetilde{\mathbf{h}}_{k,i}^j \sim \mathcal{CN}(\mathbf{0}, \mathbf{I}_{N_t})$ denotes the NLoS components, α_{ug} represents the path loss exponent associated with the UAV-user links, and κ_{ug} is the Rician factor. Similarly, the channel between the RIS and the (k,i)th user is [18]

$$\mathbf{r}_{k,i} = \sqrt{\frac{\rho_0}{\|\mathbf{w}_r - \mathbf{w}_i^k\|^{\alpha_{rg}}}}\left(\sqrt{\frac{\kappa_{rg}}{\kappa_{rg}+1}}\overline{\mathbf{r}}_{k,i} + \sqrt{\frac{1}{\kappa_{rg}+1}}\widetilde{\mathbf{r}}_{k,i}\right), \tag{5}$$

where $\overline{\mathbf{r}}_{k,i} = [1, e^{-j\frac{2\pi d}{\lambda}\cos\phi_{k,i}}, \cdots, e^{-j\frac{2\pi d(N-1)}{\lambda}\cos\phi_{k,i}}]^T$ represents the LoS component, $\cos\phi_{k,i} = \frac{x_i^k - x_r}{\|\mathbf{w}_i^k - \mathbf{w}_r\|}$ denotes the cosine of the AoD from the RIS towards the (k,i)th user, $\widetilde{\mathbf{r}}_{k,i} \sim \mathcal{CN}(\mathbf{0}, \mathbf{I}_N)$ indicates the NLoS components, α_{rg} indicates the path loss exponent associated with the RIS-user links, and κ_{rg} denotes the Rician factor.

C. NOMA transmission scheme

It is assumed that all UAVs use the same frequency resource, and each exploits NOMA technique to serve all users in its group simultaneously. In particular, the transmit signal for the kth group sent by the kth UAV is expressed as $s_k = \sum_{i=1}^{M_k}\sqrt{p_{k,i}}\tilde{s}_{k,i}$, where $p_{k,i}$ indicates the transmit power assigned to the (k,i)th user and $\tilde{s}_{k,i}$ indicates the transmit signal intended for the (k,i)th user. Let the precoding vector of the kth group be denoted by $\mathbf{f}_k \in \mathbb{C}^{N_t \times 1}, \forall k \in \mathcal{K}$. The received signal at the (k,i)th user is represented by [11]

$$\begin{aligned} y_{k,i} = &\left(\mathbf{h}_{k,i}^k + \mathbf{r}_{k,i}^H \Theta \mathbf{g}_k\right)\mathbf{f}_k\sqrt{p_{k,i}}\tilde{s}_{k,i} \\ &+ \left(\mathbf{h}_{k,i}^k + \mathbf{r}_{k,i}^H \Theta \mathbf{g}_k\right)\mathbf{f}_k \sum_{t=1, t\neq i}^{M_k}\sqrt{p_{k,t}}\tilde{s}_{k,t} \\ &+ \sum_{j=1, j\neq k}^{K}\left(\mathbf{h}_{k,i}^j + \mathbf{r}_{k,i}^H \Theta \mathbf{g}_j\right)\mathbf{f}_j \sum_{l=1}^{M_j}\sqrt{p_{j,l}}\tilde{s}_{j,l} + n_{k,i}. \end{aligned} \tag{6}$$

$n_{k,i} \sim \mathcal{CN}(0, \sigma^2)$ indicates the additive white Gaussian noise (AWGN) at the (k,i)th user.

In NOMA scheme, the decoding order of users is impacted by the effective channel gain [3]. For the RIS-assisted multi-UAV system, the effective channel gain of the combined channel depends on the placement of UAVs, RIS reflection coefficients and transmit beamforming vector, and hence we develop a dynamic-order decoding method to optimize the decoding order in the next section. Let the decoding order of the (k,i)th user and the (k,j)th user be defined as $u_k(i)$ and $u_k(j)$, where $u_k(i),\ u_k(j) \in \{1, \cdots, M_k\}$. If $\left|\left(\mathbf{h}_{k,i}^k + \mathbf{r}_{k,i}^H \Theta \mathbf{g}_k\right)\mathbf{f}_k\right|^2 < \left|\left(\mathbf{h}_{k,j}^k + \mathbf{r}_{k,j}^H \Theta \mathbf{g}_k\right)\mathbf{f}_k\right|^2$, it follows that $u_k(i) < u_k(j)$. Assuming that the decoding order in the kth group is $\left|\left(\mathbf{h}_{k,1}^k + \mathbf{r}_{k,1}^H \Theta \mathbf{g}_k\right)\mathbf{f}_k\right|^2 \leq \left|\left(\mathbf{h}_{k,2}^k + \mathbf{r}_{k,2}^H \Theta \mathbf{g}_k\right)\mathbf{f}_k\right|^2 \leq \cdots \leq \left|\left(\mathbf{h}_{k,M_k}^k + \mathbf{r}_{k,M_k}^H \Theta \mathbf{g}_k\right)\mathbf{f}_k\right|^2$. Then, the signal-to-interference-plus-noise ratio (SINR) for the (k,i)th user is given by (7). From (7), the achievable rate of the (k,i)th user is written as

$$R_{k,i} = \log_2(1 + SINR_{k,i}). \tag{8}$$

Accordingly, the sum-rate of the RIS-aided multi-UAV network is given by

$$R_{sum} = \sum_{k=1}^{K}\sum_{i=1}^{M_k} R_{k,i}. \tag{9}$$

D. Power Consumption Model and Problem Formulation

The total power consumption in the RIS-assisted multi-UAV system is composed of the transmit power $P_t = \sum_{k=1}^{K}\sum_{i=1}^{M_k} p_{k,i}$, the RIS power consumption P_{RIS} and the propulsion power of UAVs P_{UAV}, which can be given as (10) [33], [34]. Here $\widetilde{P}_0 = \frac{\hat{\delta}}{8}\varrho S_f \hat{A}\Omega^3(R_f)^3$ and $\widetilde{P}_i = (1+\hat{\kappa})\frac{\vartheta^{\frac{3}{2}}}{\sqrt{2\varrho\hat{A}}}$ are blade profile power and induced power [35]. V_f denotes the flight speed of UAVs. $\hat{\delta}$ indicates the profile drag coefficient and ϱ is air density. S_f and Ω represent rotor solidity and blade angular velocity, respectively. $\hat{A}$ denotes the rotor disc area and R_f is rotor radius. $\hat{\kappa}$ indicates incremental correction factor and ϑ is aircraft weight. U_{tip} represents tip speed and V_0 is the mean rotor induced velocity. Let P_e represent the power consumed by a reflecting unit. The power consumed by a RIS with N reflecting units can be expressed

$$SINR_{k,i}=\frac{\left|\left(\mathbf{h}_{k,i}^{k}+\mathbf{r}_{k,i}^{H}\Theta\mathbf{g}_{k}\right)\mathbf{f}_{k}\right|^{2}p_{k,i}}{\left|\left(\mathbf{h}_{k,i}^{k}+\mathbf{r}_{k,i}^{H}\Theta\mathbf{g}_{k}\right)\mathbf{f}_{k}\right|^{2}\sum_{t=i+1}^{M_k}p_{k,t}+\sum_{j=1,j\neq k}^{K}\left|\left(\mathbf{h}_{k,i}^{j}+\mathbf{r}_{k,i}^{H}\Theta\mathbf{g}_{j}\right)\mathbf{f}_{j}\right|^{2}\sum_{l=1}^{M_j}p_{j,l}+\sigma^{2}}. \tag{7}$$

$$P_{sum}=P_t+P_{RIS}+P_{UAV}=\sum_{k=1}^{K}\sum_{i=1}^{M_k}p_{k,i}+NP_e+\left(\widetilde{P}_0\left(1+\frac{3(V_f)^2}{(U_{tip})^2}\right)+\widetilde{P}_i\left(\sqrt{1+\frac{(V_f)^4}{4(V_0)^4}}-\frac{(V_f)^2}{2(V_0)^2}\right)^{\frac{1}{2}}+\frac{1}{2}\hat{d}\varrho S_f\hat{A}(V_f)^3\right). \tag{10}$$

$$P_{sum}=P_t+P_{RIS}+P_{UAV}=\sum_{k=1}^{K}\sum_{i=1}^{M_k}p_{k,i}+NP_e+\left(\widetilde{P}_0+\widetilde{P}_i\right)=\sum_{k=1}^{K}\sum_{i=1}^{M_k}p_{k,i}+NP_e+\left(\frac{\hat{\delta}}{8}\varrho S_f\hat{A}\Omega^3(R_f)^3+(1+\hat{\kappa})\frac{\vartheta^{\frac{3}{2}}}{\sqrt{2\varrho\hat{A}}}\right). \tag{11}$$

as NP_e [36]. Since the rotary-wing UAVs in this paper hover in fixed locations, the required power for UAVs is expressed as $P_h=\widetilde{P}_0+\widetilde{P}_i=\frac{\hat{\delta}}{8}\varrho S_f\hat{A}\Omega^3(R_f)^3+(1+\hat{\kappa})\frac{\vartheta^{\frac{3}{2}}}{\sqrt{2\varrho\hat{A}}}$ [35]. Here, $\widetilde{P}_0$ and $\widetilde{P}_i$ are all constants. As a result, (10) can be represented as (11). Next, we concentrate on the joint optimization of the UAV's position $\mathbf{q}=\{\mathbf{q}_k,\forall k\in\mathcal{K}\}$, RIS reflection matrix Θ, transmit power $\mathbf{P}=\{p_{k,i},\forall k\in\mathcal{K},i\in\mathcal{M}_k\}$, transmit beamforming vector $\mathbf{F}=\{\mathbf{f}_k,\forall k\in\mathcal{K}\}$ and decoding order $\mathbf{u}=\{u_k(i),\forall k\in\mathcal{K},i\in\mathcal{M}_k\}$ so as to minimize the overall power consumption under minimum rate constraints for users and the minimum distance between UAVs. Mathematically, the power minimization problem is formulated as

$$(\text{P1}):\min_{\mathbf{q},\Theta,\mathbf{P},\mathbf{F},\mathbf{u}}\ P_{sum}=P_t+P_{RIS}+P_{UAV} \tag{12a}$$
$$\text{s.t. } p_{k,i}\geq 0, \tag{12b}$$
$$\log_2(1+SINR_{k,i})\geq R_{min}, \tag{12c}$$
$$\|\mathbf{q}_k-\mathbf{q}_j\|^2\geq\Delta_{min}^2,\forall k\neq j\in\mathcal{K}, \tag{12d}$$
$$\theta_n\in[0,2\pi),\forall n\in\{1,\cdots,N\}, \tag{12e}$$
$$\mathbf{u}\in\mathcal{D}, \tag{12f}$$
$$u_k(i)>u_k(t),\text{if}\left\|\mathbf{h}_{k,i}^{k}+\mathbf{r}_{k,i}^{H}\Theta\mathbf{g}_{k}\right\|^2>\left\|\mathbf{h}_{k,t}^{k}+\mathbf{r}_{k,t}^{H}\Theta\mathbf{g}_{k}\right\|^2,$$
$$u_k(i)<u_k(t),\text{if}\left\|\mathbf{h}_{k,i}^{k}+\mathbf{r}_{k,i}^{H}\Theta\mathbf{g}_{k}\right\|^2=\left\|\mathbf{h}_{k,t}^{k}+\mathbf{r}_{k,t}^{H}\Theta\mathbf{g}_{k}\right\|^2,$$
$$\|\mathbf{w}_r-\mathbf{w}_t^k\|^2\leq\|\mathbf{w}_r-\mathbf{w}_i^k\|^2, \tag{12g}$$
$$\|\mathbf{f}_k\|^2=1. \tag{12h}$$

Constraint (12b) is the transmit power constraints of the UAVs. In constraint (12c), R_{min} represents the rate threshold which specifies the minimum rate requirements for each user. Constraint (12d) is imposed such that the inter-UAV distance cannot exceed the minimum inter-UAV distance Δ_{min}. Constraints (12f) and (12g) correspond to the constraints on the NOMA decoding order, where $\mathcal{D}$ indicates the set of all feasible decoding orders. Constraint (12h) represents the boundary constraint for the precoding vector. Problem (P1) is non-convex owning to the coupling variables, and thus is hard to solve via the standard convex optimization techniques [37]. In the next section, we develop a joint UAV deployment and resource allocation algorithm to tackle (P1), which is based on the SCA method and the Gaussian randomization procedure.

III. Joint UAV Deployment and Resource Allocation Algorithm

In this section, in order to solve the aforementioned coupled non-convex problem, we divide the resultant optimization problem into four independent subproblems, and optimize the positions of UAVs, active beamforming vectors, RIS reflection coefficients, transmit power and decoding order iteratively. Since the passive beamforming optimization needs to obtain the path loss coefficients and the beam-scanning angles, the positions of UAVs and the active beamforming vectors are optimized first. Subsequently, based on the UAV placement optimization and the active beamforming design, the RIS reflection coefficients are optimized to maximize the channel power gain. Then, with the fixed variables, the transmit power is optimized according to the NOMA schemes. Finally, based on the combined channel power gain, the decoding order is optimized to ensure fairness among users and further reduce the power consumption.

A. Joint UAV Deployment and Active Beamforming Design

For any given Θ, $\mathbf{P}$ and $\mathbf{u}$, it is shown that the MRT can be applied to perform the active beamforming design [19]; furthermore, the active beamforming vector for the kth group is written as

$$\mathbf{f}_k^*=\frac{\left(\mathbf{h}_{k,i}^{k}+\mathbf{r}_{k,i}^{H}\Theta\mathbf{g}_{k}\right)^{H}}{\|\mathbf{h}_{k,i}^{k}+\mathbf{r}_{k,i}^{H}\Theta\mathbf{g}_{k}\|},\forall k\in\mathcal{K},i\in\mathcal{M}_k. \tag{13}$$

From (13), the achievable rate in (8) is then represented by (14). Here, $C_{k,i}^{j}=\left\|\mathbf{h}_{k,i}^{j}+\mathbf{r}_{k,i}^{H}\Theta\mathbf{g}_{j}\right\|^2$ represents the composite channel power gain from the jth UAV to the (k,i)th user.

Using (13) and (14), (P1) can be written as

$$(\text{P2}):\min_{\mathbf{q}}\ P_{sum} \tag{15a}$$
$$\text{s.t. } R_{k,i}\geq R_{min}, \tag{15b}$$
$$\|\mathbf{q}_k-\mathbf{q}_j\|^2\geq\Delta_{min}^2,\forall k\neq j\in\mathcal{K}. \tag{15c}$$

Problem (P2) is non-convex due to constraints (15b) and (15c). Since $\{R_{k,i}\}$ in constraint (15b) are random variables, it is

$$R_{k,i}=\log_2\left(1+\frac{\left\|\mathbf{h}_{k,i}^k+\mathbf{r}_{k,i}^H\Theta\mathbf{g}_k\right\|^2 p_{k,i}}{\left\|\mathbf{h}_{k,i}^k+\mathbf{r}_{k,i}^H\Theta\mathbf{g}_k\right\|^2\sum_{t=i+1}^{M_k}p_{k,t}+\sum_{j=1,j\neq k}^{K}\left\|\mathbf{h}_{k,i}^j+\mathbf{r}_{k,i}^H\Theta\mathbf{g}_j\right\|^2\sum_{l=1}^{M_j}p_{j,l}+\sigma^2}\right). \tag{14}$$

challenging to achieve the optimal solutions for (P2). For convenience of analysis, we consider the expected achievable rate, and constraint (15b) is modified as [38]

$$\mathbb{E}\{R_{k,i}\}\geq R_{min}. \tag{16}$$

It can be shown that the closed-form solution for $\mathbb{E}\{R_{k,i}\}$ is still hard to derive. To overcome this issue, we convert $\mathbb{E}\{R_{k,i}\}$ into a convex function via the following propositions.

Proposition 1: Let X and Y denote two independent positive random variables. Then, for any $\mu,\nu>0$, it holds that

$$\mathbb{E}\left\{\log_2\left(1+\frac{\mu}{\nu+\frac{X}{Y}}\right)\right\}\approx\mathbb{E}\left\{\log_2\left(1+\frac{\mu}{\nu+\frac{\mathbb{E}\{X\}}{\mathbb{E}\{Y\}}}\right)\right\}. \tag{17}$$

Proof: Please see [38] for the proof of Proposition 1. ■

Proposition 2: The expected value of the composite channel power gain from the jth UAV to the (k,i)th user can be formulated as

$$\mathbb{E}\{C_{k,i}^j\}\triangleq\omega_{k,i}^j=\left\|\widehat{\mathbf{h}}_{k,i}^j+\widehat{\mathbf{r}}_{k,i}^H\Theta\mathbf{g}_j\right\|^2+\frac{(\rho_0-\gamma_{ug})N_t}{\|\mathbf{q}_j-\mathbf{w}_i^k\|^{\alpha_{ug}}}+\frac{\eta_{k,i}}{\|\mathbf{q}_j-\mathbf{w}_r\|^2}, \tag{18}$$

where $\widehat{\mathbf{h}}_{k,i}^j=\sqrt{\frac{\gamma_{ug}}{\|\mathbf{q}_j-\mathbf{w}_i^k\|^{\alpha_{ug}}}}\overline{\mathbf{h}}_{k,i}^j$, $\widehat{\mathbf{r}}_{k,i}^H=\sqrt{\frac{\gamma_{rg}}{\|\mathbf{w}_r-\mathbf{w}_i^k\|^{\alpha_{rg}}}}\overline{\mathbf{r}}_{k,i}^H$, $\eta_{k,i}=\frac{NN_t\rho_0(\rho_0-\gamma_{rg})}{\|\mathbf{w}_r-\mathbf{w}_i^k\|^{\alpha_{rg}}}$, $\gamma_{ug}=\frac{\kappa_{ug}\rho_0}{\kappa_{ug}+1}$ and $\gamma_{rg}=\frac{\kappa_{rg}\rho_0}{\kappa_{rg}+1}$.

Proof: Please see Appendix A for the proof of Proposition 2. ■

Using (17) and (18), we transform $\mathbb{E}\{R_{k,i}\},\forall k\in\mathcal{K},i\in\mathcal{M}_k$ as

$$\begin{aligned}&\mathbb{E}\{R_{k,i}\}\\&\approx\mathbb{E}\left\{\log_2\left(1+\frac{p_{k,i}}{\sum_{t=i+1}^{M_k}p_{k,t}+\frac{\sum_{j=1,j\neq k}^{K}\mathbb{E}\{C_{k,i}^j\}\sum_{l=1}^{M_j}p_{j,l}+\sigma^2}{\mathbb{E}\{C_{k,i}^k\}}}\right)\right\}\\&=\log_2\left(1+\frac{p_{k,i}}{\sum_{t=i+1}^{M_k}p_{k,t}+\frac{\sum_{j=1,j\neq k}^{K}\omega_{k,i}^j\sum_{l=1}^{M_j}p_{j,l}+\sigma^2}{\omega_{k,i}^k}}\right)\triangleq\widetilde{R}_{k,i}.\end{aligned} \tag{22}$$

Equation (22) is still a non-convex function owning to the coupled variables. To overcome this problem, we first add a set of supplementary variables. Let the upper bound of the Euclidean distance between the UAV and its connected users be defined as $\{up_{k,i}^k,\forall i\in\mathcal{M}_k,k\in\mathcal{K}\}$. Let $\{lp_{k,i}^j,\forall i\in\mathcal{M}_k,j\neq k\in\mathcal{K}\}$ be the lower bound of the Euclidean distance between the UAV and its unconnected users. Here, $up_{k,i}^k>0$. Let the upper bound and the lower bound of the direct distance between the UAV and the RIS be denoted as $\{ub_k,\forall k\in\mathcal{K}\}$ and $\{lb_k>0,\forall k\in\mathcal{K}\}$. Thus, we have

$$\left(up_{k,i}^k\right)^2\geq\|\mathbf{q}_k-\mathbf{w}_i^k\|^2,\forall i\in\mathcal{M}_k,k\in\mathcal{K}, \tag{23a}$$

$$\|\mathbf{q}_j-\mathbf{w}_i^k\|^2\geq\left(lp_{k,i}^j\right)^2,\forall i\in\mathcal{M}_k,j\neq k\in\mathcal{K}, \tag{23b}$$

$$\left(ub_k\right)^2\geq\|\mathbf{q}_k-\mathbf{w}_r\|^2,\forall k\in\mathcal{K}, \tag{23c}$$

$$\|\mathbf{q}_k-\mathbf{w}_r\|^2\geq\left(lb_k\right)^2,\forall k\in\mathcal{K}. \tag{23d}$$

By substituting (23) into (18), it can be reformulated as (24) and (25). Here, $\{\underline{\omega}_{k,i}^k,\forall i\in\mathcal{M}_k,k\in\mathcal{K}\}$ and $\{\overline{\omega}_{k,i}^j,\forall i\in\mathcal{M}_k,j\neq k\in\mathcal{K}\}$ are the lower bound of $\omega_{k,i}^k$ and the upper bound of $\omega_{k,i}^j$. $A_{k,i}^k=\rho_0\|\widehat{\mathbf{r}}_{k,i}^H\Theta\bar{\mathbf{g}}_k^T\tilde{\mathbf{g}}_k\|^2+\eta_{k,i}$, $B_{k,i}^k=2\mathrm{Re}\left\{\sqrt{\gamma_{ug}\rho_0}\widehat{\mathbf{r}}_{k,i}^H\Theta\bar{\mathbf{g}}_k^T\tilde{\mathbf{g}}_k\left(\overline{\mathbf{h}}_{k,i}^k\right)^H\right\}$, $D_{k,i}^j=\rho_0\|\widehat{\mathbf{r}}_{k,i}^H\Theta\bar{\mathbf{g}}_j^T\tilde{\mathbf{g}}_j\|^2+\eta_{k,i}$ and $E_{k,i}^j=2\mathrm{Re}\left\{\sqrt{\gamma_{ug}\rho_0}\widehat{\mathbf{r}}_{k,i}^H\Theta\bar{\mathbf{g}}_j^T\tilde{\mathbf{g}}_j\left(\overline{\mathbf{h}}_{k,i}^j\right)^H\right\}$. Let $(U_{k,i})^2=\sum_{j=1,j\neq k}^{K}\overline{\omega}_{k,i}^j\sum_{l=1}^{M_j}p_{j,l}+\sigma^2$ and $\tau_{k,i}=\sum_{t=i+1}^{M_K}p_{k,t}+\frac{(U_{k,i})^2}{\underline{\omega}_{k,i}^k}$. It then follows that the lower bound of $\widetilde{R}_{k,i}$ is written as

$$\widetilde{R}_{k,i}\geq\log_2\left(1+\frac{p_{k,i}}{\tau_{k,i}}\right),\forall i\in\mathcal{M}_k,k\in\mathcal{K}. \tag{26}$$

Using (16) and (23)-(26), (P2) is rewritten as the following problem

$$(\mathrm{P2.1}):\min_{\mathbf{q},\mathbf{x}}\ P_{sum} \tag{27a}$$

$$\text{s.t. }\log_2\left(1+\frac{p_{k,i}}{\tau_{k,i}}\right)\geq R_{min}, \tag{27b}$$

$$\tau_{k,i}\geq\sum_{t=i+1}^{M_k}p_{k,t}+\frac{(U_{k,i})^2}{\underline{\omega}_{k,i}^k}, \tag{27c}$$

$$(U_{k,i})^2\geq\sum_{j=1,j\neq k}^{K}\overline{\omega}_{k,i}^j\sum_{l=1}^{M_j}p_{j,l}+\sigma^2, \tag{27d}$$

$$\underline{\omega}_{k,i}^k\leq\rho_0N_t(up_{k,i}^k)^{-\alpha_{ug}}+A_{k,i}^k(ub_k)^{-2}+B_{k,i}^k(up_{k,i}^k)^{-\alpha_{ug}/2}(ub_k)^{-1}, \tag{27e}$$

$$\overline{\omega}_{k,i}^j\geq\rho_0N_t(lp_{k,i}^j)^{-\alpha_{ug}}+D_{k,i}^j(lb_j)^{-2}+E_{k,i}^j(lp_{k,i}^j)^{-\alpha_{ug}/2}(lb_j)^{-1}, \tag{27f}$$

$$\|\mathbf{q}_k-\mathbf{q}_j\|^2\geq\Delta_{min}^2, \tag{27g}$$

$$\left(up_{k,i}^k\right)^2\geq\|\mathbf{q}_k-\mathbf{w}_i^k\|^2, \tag{27h}$$

$$\|\mathbf{q}_j-\mathbf{w}_i^k\|^2\geq\left(lp_{k,i}^j\right)^2, \tag{27i}$$

$$\left(ub_k\right)^2\geq\|\mathbf{q}_k-\mathbf{w}_r\|^2, \tag{27j}$$

$$\|\mathbf{q}_k-\mathbf{w}_r\|^2\geq\left(lb_k\right)^2, \tag{27k}$$

where $\mathbf{x}=\{\tau_{k,i},U_{k,i},\underline{\omega}_{k,i}^k,\overline{\omega}_{k,i}^j,up_{k,i}^k,ub_k,lp_{k,i}^j,lb_k,\forall j\neq k\in\mathcal{K},i\in\mathcal{M}_k\}$. (P2.1) is obviously non-convex owning to the non-convex constraints (27d)-(27k). Next, SCA [39] is

$$\underline{\omega}_{k,i}^{k} = \left\| \sqrt{\gamma_{ug}(up_{k,i}^{k})^{-\alpha_{ug}}}\overline{\mathbf{h}}_{k,i}^{k} + \sqrt{\rho_0(ub_k)^{-2}}\widehat{\mathbf{r}}_{k,i}^{H}\Theta\bar{\mathbf{g}}_k^T\tilde{\mathbf{g}}_k \right\|^2 + (\rho_0-\gamma_{ug})N_t(up_{k,i}^{k})^{-\alpha_{ug}} + \eta_{k,i}(ub_k)^{-2}$$
$$= \rho_0 N_t(up_{k,i}^{k})^{-\alpha_{ug}} + A_{k,i}^{k}(ub_k)^{-2} + B_{k,i}^{k}(up_{k,i}^{k})^{-\alpha_{ug}/2}(ub_k)^{-1}. \quad (24)$$

$$\overline{\omega}_{k,i}^{j} = \left\| \sqrt{\gamma_{ug}(lp_{k,i}^{j})^{-\alpha_{ug}}}\overline{\mathbf{h}}_{k,i}^{j} + \sqrt{\rho_0(lb_j)^{-2}}\widehat{\mathbf{r}}_{k,i}^{H}\Theta\bar{\mathbf{g}}_j^T\tilde{\mathbf{g}}_j \right\|^2 + (\rho_0-\gamma_{ug})N_t(lp_{k,i}^{j})^{-\alpha_{ug}} + \eta_{k,i}(lb_j)^{-2}$$
$$= \rho_0 N_t(lp_{k,i}^{j})^{-\alpha_{ug}} + D_{k,i}^{j}(lb_j)^{-2} + E_{k,i}^{j}(lp_{k,i}^{j})^{-\alpha_{ug}/2}(lb_j)^{-1}. \quad (25)$$

exploited to achieve a suboptimal solution of (P2.1). From (27b), since the left side $\log_2\left(1+\frac{p_{k,i}}{\tau_{k,i}}\right)$ is a concave function in regard to $\tau_{k,i}$, the first-order Taylor expansion is employed to obtain a global upper bound on the achievable data rate [37]. Define $e(\{\tau_{k,i}\})$ as $\log_2\left(1+\frac{p_{k,i}}{\tau_{k,i}}\right)$. For a given $\{\tau_{k,i}^{(m)}\}$ in the mth iteration, we have

$$e(\{\tau_{k,i}\}) \le \log_2\left(1+\frac{p_{k,i}}{\tau_{k,i}^{(m)}}\right) - \frac{p_{k,i}}{\left(\tau_{k,i}^{(m)}+p_{k,i}\right)\tau_{k,i}^{(m)}\ln 2}\left(\tau_{k,i}-\tau_{k,i}^{(m)}\right). \quad (28)$$

Using (28), (27b) can be reformulated as

$$\log_2\left(1+\frac{p_{k,i}}{\tau_{k,i}^{(m)}}\right) - \frac{p_{k,i}}{\left(\tau_{k,i}^{(m)}+p_{k,i}\right)\tau_{k,i}^{(m)}\ln 2}\left(\tau_{k,i}-\tau_{k,i}^{(m)}\right) \ge R_{min}. \quad (29)$$

Similarly, the lower bound on the left hand side of constraints (27d), (27g)-(27k) are given by

$$\left(U_{k,i}^{(m)}\right)^2 + 2U_{k,i}^{(m)}\left(U_{k,i}-U_{k,i}^{(m)}\right) \ge \sum_{j=1,j\neq k}^{K}\overline{\omega}_{k,i}^{j}\sum_{l=1}^{M_j}p_{j,l}+\sigma^2, \quad (30a)$$

$$-\left\|\mathbf{q}_k^{(m)}-\mathbf{q}_j^{(m)}\right\|^2 + 2\left(\mathbf{q}_k^{(m)}-\mathbf{q}_j^{(m)}\right)^T(\mathbf{q}_k-\mathbf{q}_j) \ge \Delta_{min}^2, \quad (30b)$$

$$\left(up_{k,i}^{k(m)}\right)^2 + 2up_{k,i}^{k(m)}\left(up_{k,i}^{k}-up_{k,i}^{k(m)}\right) \ge \|\mathbf{q}_k-\mathbf{w}_i^k\|^2, \quad (30c)$$

$$\|\mathbf{q}_j^{(m)}-\mathbf{w}_i^k\|^2 + 2(\mathbf{q}_j^{(m)}-\mathbf{w}_i^k)^T(\mathbf{q}_j-\mathbf{q}_j^{(m)}) \ge \left(lp_{k,i}^{j}\right)^2, \quad (30d)$$

$$\left(ub_k^{(m)}\right)^2 + 2ub_k^{(m)}\left(ub_k-ub_k^{(m)}\right) \ge \|\mathbf{q}_k-\mathbf{w}_r\|^2, \quad (30e)$$

$$\|\mathbf{q}_k^{(m)}-\mathbf{w}_r\|^2 + 2\left(\mathbf{q}_k^{(m)}-\mathbf{w}_r\right)^T\left(\mathbf{q}_k-\mathbf{q}_k^{(m)}\right) \ge (lb_k)^2. \quad (30f)$$

For the non-convex constraints (27e) and (27f), the AoAs and AoDs are affected by the position of UAVs. Consequently, $\bar{\mathbf{g}}_k$ and $\tilde{\mathbf{g}}_k$ are updated at each iteration, complicating the solution of the original problem. To address this problem, let $\{\mathbf{q}_k^{(m)}, \forall k\in\mathcal{K}\}$ be the position of the kth UAV in the mth iteration, we consider the following constraints

$$\left\|\mathbf{q}_k-\mathbf{q}_k^{(m)}\right\|^2 \le \delta^2, \forall k\in\mathcal{K}, \quad (31)$$

where $\delta \le H\varepsilon_{max}$ indicates the relative displacement of the kth UAV during the mth iteration and $\varepsilon_{max}>0$. Because the value of δ is sufficiently small, the AoAs and AoDs are assumed to be almost unchanged during each iteration [26]. In this case, the value of $\{A_{k,i}^k, B_{k,i}^k, D_{k,i}^j, E_{k,i}^j\}$ is nearly unchanged, and thus the horizontal position of UAVs in the $(m+1)$th iteration can be designed through the AoAs acquired in the mth iteration [33]. This implies that constraints (27e) and (27f) are determined by $\{up_{k,i}^k, lp_{k,i}^j, ub_k, lb_k\}$. Using the above assumptions and let $\widetilde{f}_{k,i}^k = \rho_0 N_t(up_{k,i}^k)^{-\alpha_{ug}} + A_{k,i}^k(ub_k)^{-2}$, $\widetilde{g}_{k,i}^k = (up_{k,i}^k)^{-\alpha_{ug}/2}(ub_k)^{-1}$, the right hand side of (27e) can be expressed as $\widetilde{f}_{k,i}^k + B_{k,i}^k\widetilde{g}_{k,i}^k$. Note that $\widetilde{f}_{k,i}^k$ and $\widetilde{g}_{k,i}^k$ are convex [26]. Here, if $B_{k,i}^k \ge 0$, it follows that $\widetilde{f}_{k,i}^k + |B_{k,i}^k|\,\widetilde{g}_{k,i}^k$ is a convex function; otherwise, it follows that $\widetilde{f}_{k,i}^k - |B_{k,i}^k|\,\widetilde{g}_{k,i}^k$ is a difference of convex (DC) function. Then, the lower bound of $\widetilde{f}_{k,i}^k + B_{k,i}^k\widetilde{g}_{k,i}^k$ can be obtained via the first-order Taylor expansion

$$\left[\widetilde{f}_{k,i}^k + B_{k,i}^k\widetilde{g}_{k,i}^k\right]^{lb} = \begin{cases} \left[\widetilde{f}_{k,i}^k\right]^{lb} + |B_{k,i}^k|\left[\widetilde{g}_{k,i}^k\right]^{lb}, B_{k,i}^k \ge 0, \\ \left[\widetilde{f}_{k,i}^k\right]^{lb} - |B_{k,i}^k|\,\widetilde{g}_{k,i}^k, B_{k,i}^k < 0, \end{cases} \quad (32)$$

$$\left[\widetilde{f}_{k,i}^k\right]^{lb} = \rho_0 N_t\left(up_{k,i}^{k(m)}\right)^{-\alpha_{ug}} - \alpha_{ug}\rho_0 N_t\left(up_{k,i}^{k(m)}\right)^{-\alpha_{ug}-1}\left(up_{k,i}^k - up_{k,i}^{k(m)}\right) + A_{k,i}^k\left(ub_k^{(m)}\right)^{-2} - 2A_{k,i}^k\left(ub_k^{(m)}\right)^{-3}\left(ub_k-ub_k^{(m)}\right), \quad (33)$$

$$\left[\widetilde{g}_{k,i}^k\right]^{lb} = \left(up_{k,i}^{k(m)}\right)^{-\alpha_{ug}/2}\left(ub_k^{(m)}\right)^{-1} - \frac{\alpha_{ug}}{2}\left(up_{k,i}^{k(m)}\right)^{-\alpha_{ug}/2-1}\left(ub_k^{(m)}\right)^{-1}\left(up_{k,i}^k - up_{k,i}^{k(m)}\right) - \left(up_{k,i}^{k(m)}\right)^{-\alpha_{ug}/2}\left(ub_k^{(m)}\right)^{-2}\left(ub_k-ub_k^{(m)}\right). \quad (34)$$

Similarly, let $\widetilde{f}_{k,i}^j = \rho_0 N_t(lp_{k,i}^j)^{-\alpha_{ug}} + D_{k,i}^j(lb_j)^{-2}$, $\widetilde{g}_{k,i}^j = \left(lp_{k,i}^j\right)^{-\alpha_{ug}/2}(lb_j)^{-1}$. The upper bound of $\widetilde{f}_{k,i}^j + E_{k,i}^j\widetilde{g}_{k,i}^j$ can then be expressed as

$$\left[\widetilde{f}_{k,i}^j + E_{k,i}^j\widetilde{g}_{k,i}^j\right]^{ub} = \begin{cases} \widetilde{f}_{k,i}^j + |E_{k,i}^j|\,\widetilde{g}_{k,i}^j, E_{k,i}^j \ge 0, \\ \widetilde{f}_{k,i}^j - |E_{k,i}^j|\left[\widetilde{g}_{k,i}^j\right]^{lb}, E_{k,i}^j < 0, \end{cases} \quad (35)$$

where

$$\begin{aligned}\left[\widetilde{g}_{k,i}^{j}\right]^{lb} &= \left(lp_{k,i}^{j(m)}\right)^{-\alpha_{ug}/2}\left(lb_{j}^{(m)}\right)^{-1} \\ &- \frac{\alpha_{ug}}{2}\left(lp_{k,i}^{j(m)}\right)^{-\alpha_{ug}/2-1}\left(lb_{j}^{(m)}\right)^{-1}\left(lp_{k,i}^{j}-lp_{k,i}^{j(m)}\right) \\ &- \left(lp_{k,i}^{j(m)}\right)^{-\alpha_{ug}/2}\left(lb_{j}^{(m)}\right)^{-2}\left(lb_{j}-lb_{j}^{(m)}\right). \end{aligned} \tag{36}$$

Substituting (29)-(36) into problem (P2.1), problem (P2.1) is reformulated as

$$(\text{P2.2}): \min_{\mathbf{q},\mathbf{x}} \ P_{sum} \tag{37a}$$

$$\text{s.t. } \log_2\left(1+\frac{p_{k,i}}{\tau_{k,i}^{(m)}}\right) - \frac{p_{k,i}}{\left(\tau_{k,i}^{(m)}+p_{k,i}\right)\tau_{k,i}^{(m)}\ln 2}\left(\tau_{k,i}-\tau_{k,i}^{(m)}\right) \geq R_{min}, \tag{37b}$$

$$\tau_{k,i} \geq \sum_{t=i+1}^{M_k} p_{k,t} + \frac{(U_{k,i})^2}{\underline{\omega}_{k,i}^{k}}, \tag{37c}$$

$$\left(U_{k,i}^{(m)}\right)^2 + 2U_{k,i}^{(m)}\left(U_{k,i}-U_{k,i}^{(m)}\right) \geq \sum_{j=1,j\neq k}^{K}\overline{\omega}_{k,i}^{j}\sum_{l=1}^{M_j} p_{j,l}+\sigma^2, \tag{37d}$$

$$-\left\|\mathbf{q}_{k}^{(m)}-\mathbf{q}_{j}^{(m)}\right\|^2 + 2\left(\mathbf{q}_{k}^{(m)}-\mathbf{q}_{j}^{(m)}\right)^T(\mathbf{q}_k-\mathbf{q}_j) \geq \Delta_{min}^2, \tag{37e}$$

$$\left(up_{k,i}^{k(m)}\right)^2 + 2up_{k,i}^{k(m)}\left(up_{k,i}^{k}-up_{k,i}^{k(m)}\right) \geq \|\mathbf{q}_k-\mathbf{w}_i^k\|^2, \tag{37f}$$

$$\|\mathbf{q}_{j}^{(m)}-\mathbf{w}_i^k\|^2 + 2(\mathbf{q}_{j}^{(m)}-\mathbf{w}_i^k)^T(\mathbf{q}_j-\mathbf{q}_j^{(m)}) \geq \left(lp_{k,i}^{j}\right)^2, \tag{37g}$$

$$\left(ub_{k}^{(m)}\right)^2 + 2ub_{k}^{(m)}\left(ub_k-ub_{k}^{(m)}\right) \geq \|\mathbf{q}_k-\mathbf{w}_r\|^2, \tag{37h}$$

$$\|\mathbf{q}_{k}^{(m)}-\mathbf{w}_r\|^2 + 2\left(\mathbf{q}_{k}^{(m)}-\mathbf{w}_r\right)^T\left(\mathbf{q}_k-\mathbf{q}_{k}^{(m)}\right) \geq \left(lb_k\right)^2, \tag{37i}$$

$$\left\|\mathbf{q}_k-\mathbf{q}_{k}^{(m)}\right\|^2 \leq \delta^2, \tag{37j}$$

$$\underline{\omega}_{k,i}^{k} \leq \left[\widetilde{f}_{k,i}^{k}+B_{k,i}^{k}\widetilde{g}_{k,i}^{k}\right]^{lb}, \tag{37k}$$

$$\overline{\omega}_{k,i}^{j} \geq \left[\widetilde{f}_{k,i}^{j}+E_{k,i}^{j}\widetilde{g}_{k,i}^{j}\right]^{ub}. \tag{37l}$$

Problem (P2.2) ia a convex optimization problem, and hence can be tackled through the effective convex optimization approaches [37].

B. RIS Phase Shift Matrix Design

With a fixed $\mathbf{q}$, $\mathbf{P}$, $\mathbf{u}$ and considering (14) and (22), (P1) is equivalently expressed as

$$(\text{P3}): \min_{\Theta} \ P_{sum} \tag{38a}$$

$$\text{s.t. } \theta_n \in [0,2\pi), \forall n \in \{1,\cdots,N\}, \tag{38b}$$

$$\log_2\left(1+\frac{p_{k,i}}{\sum_{t=i+1}^{M_k}p_{k,t}+\frac{\sum_{j=1,j\neq k}^{K}\omega_{k,i}^{j}\sum_{l=1}^{M_j}p_{j,l}+\sigma^2}{\omega_{k,i}^{k}}}\right) \geq R_{min}. \tag{38c}$$

(P3) is non-convex owning to the constraint (38c). Thus, we convert problem (P3) into a convex optimization problem by using algebraic transformations. We first define $a_{k,i}^{j} = \text{diag}\left(\widehat{\mathbf{r}}_{k,i}^{H}\right)\mathbf{g}_j$, $\tilde{\mathbf{u}} = [\mu_1,\cdots,\mu_n,\cdots,\mu_N]^H$, $\mu_n = e^{j\theta_n}$, $\bar{\mathbf{u}} = [\tilde{\mathbf{u}};1]$ and $\mathbf{V} = \bar{\mathbf{u}}\bar{\mathbf{u}}^H$. Next, we introduce a new complex matrix $\mathcal{R}_{k,i}^{j} = \left[a_{k,i}^{j}(a_{k,i}^{j})^H, a_{k,i}^{j}(\widehat{\mathbf{h}}_{k,i}^{j})^H; (a_{k,i}^{j})^H\widehat{\mathbf{h}}_{k,i}^{j}, 0\right]$ associated with the RIS phase shift matrix $\mathbf{V}$ as

$$\mathcal{R}_{k,i}^{j}\mathbf{V} = \begin{bmatrix} a_{k,i}^{j}(a_{k,i}^{j})^H\tilde{\mathbf{u}}\tilde{\mathbf{u}}^H + a_{k,i}^{j}(\widehat{\mathbf{h}}_{k,i}^{j})^H\tilde{\mathbf{u}}^H, a_{k,i}^{j}(a_{k,i}^{j})^H\tilde{\mathbf{u}} + (a_{k,i}^{j})^H(\widehat{\mathbf{h}}_{k,i}^{j})^H \\ (a_{k,i}^{j})^H\widehat{\mathbf{h}}_{k,i}^{j}\tilde{\mathbf{u}}\tilde{\mathbf{u}}^H, (a_{k,i}^{j})^H\widehat{\mathbf{h}}_{k,i}^{j}\tilde{\mathbf{u}} \end{bmatrix}. \tag{39}$$

Note that $\text{tr}(\mathcal{R}_{k,i}^{j}\mathbf{V}) = a_{k,i}^{j}(a_{k,i}^{j})^H\tilde{\mathbf{u}}\tilde{\mathbf{u}}^H + a_{k,i}^{j}(\widehat{\mathbf{h}}_{k,i}^{j})^H\tilde{\mathbf{u}}^H + (a_{k,i}^{j})^H\widehat{\mathbf{h}}_{k,i}^{j}\tilde{\mathbf{u}}$. Then, from (18) and (39), it follows that

$$\|\widehat{\mathbf{h}}_{k,i}^{j}+\widehat{\mathbf{r}}_{k,i}^{H}\Theta\mathbf{g}_j\|^2 = \text{tr}(\mathcal{R}_{k,i}^{j}\mathbf{V}) + \|\widehat{\mathbf{h}}_{k,i}^{j}\|^2, \tag{40}$$

$$\mathbb{E}\{C_{k,i}^{j}\} = \text{tr}(\mathcal{R}_{k,i}^{j}\mathbf{V}) + \|\widehat{\mathbf{h}}_{k,i}^{j}\|^2 + \frac{(\rho_0-\gamma_{ug})N_t}{\|\mathbf{q}_j-\mathbf{w}_i^k\|^{\alpha_{ug}}} + \frac{\eta_{k,i}}{\|\mathbf{q}_j-\mathbf{w}_r\|^2}. \tag{41}$$

Furthermore, by defining $\Gamma_{k,i}^{j} = \|\widehat{\mathbf{h}}_{k,i}^{j}\|^2 + \frac{(\rho_0-\gamma_{ug})N_t}{\|\mathbf{q}_j-\mathbf{w}_i^k\|^{\alpha_{ug}}} + \frac{\eta_{k,i}}{\|\mathbf{q}_j-\mathbf{w}_r\|^2}$ and considering (40)-(41), $\widetilde{R}_{k,i}$ can be reformulated as (42). Using the above transformations and let $\widetilde{\beta}_{k,i} = \sum_{t=i}^{M_k}\Gamma_{k,i}^{k}p_{k,t} + \sum_{j=1,j\neq k}^{K}\Gamma_{k,i}^{j}\sum_{l=1}^{M_j}p_{j,l}+\sigma^2$, $\overline{\beta}_{k,i} = \sum_{t=i+1}^{M_k}\Gamma_{k,i}^{k}p_{k,t} + \sum_{j=1,j\neq k}^{K}\Gamma_{k,i}^{j}\sum_{l=1}^{M_j}p_{j,l}+\sigma^2$, (42) can be equivalently expressed as

$$\begin{aligned}\widetilde{R}_{k,i} = &\underbrace{\log_2\left(\text{tr}(\mathcal{R}_{k,i}^{k}\mathbf{V})\sum_{t=i}^{M_k}p_{k,t} + \sum_{j=1,j\neq k}^{K}\sum_{l=1}^{M_j}\text{tr}(\mathcal{R}_{k,i}^{j}\mathbf{V})p_{j,l}+\widetilde{\beta}_{k,i}\right)}_{\widehat{f}_{k,i}} \\ &- \underbrace{\log_2\left(\text{tr}(\mathcal{R}_{k,i}^{k}\mathbf{V})\sum_{t=i+1}^{M_k}p_{k,t} + \sum_{j=1,j\neq k}^{K}\sum_{l=1}^{M_j}\text{tr}(\mathcal{R}_{k,i}^{j}\mathbf{V})p_{j,l}+\overline{\beta}_{k,i}\right)}_{\widehat{g}_{k,i}}. \end{aligned} \tag{43}$$

Considering the RIS phase shift matrix $\mathbf{V} = \bar{\mathbf{u}}\bar{\mathbf{u}}^H$ and (43), (P3) is then reformulated as

$$(\text{P3.1}): \min_{\mathbf{V}} \ P_{sum} \tag{44a}$$

$$\text{s.t. } \widehat{f}_{k,i} - \widehat{g}_{k,i} \geq R_{min}, \tag{44b}$$

$$[\mathbf{V}]_{nn} = 1, n = 1,2,\cdots,N+1, \tag{44c}$$

$$\mathbf{V} \succeq 0, \tag{44d}$$

$$\text{rank}(\mathbf{V}) = 1. \tag{44e}$$

Problem (P3.1) is obviously non-convex owning to the DC function $\widehat{f}_{k,i} - \widehat{g}_{k,i}$ and the rank-one constraint. To address this issue, we first employ the SCA technique to compute the upper bound of $\widehat{g}_{k,i}$, such that (44b) can be reformulated as a

$$\widetilde{R}_{k,i} = \log_2\left(1+\frac{p_{k,i}}{\sum_{t=i+1}^{M_k} p_{k,t}+\frac{\sum_{j=1,j\neq k}^{K}(\mathrm{tr}(\mathcal{R}_{k,i}^{j}\mathbf{V})+\Gamma_{k,i}^{j})\sum_{l=1}^{M_j} p_{j,l}+\sigma^2}{\mathrm{tr}(\mathcal{R}_{k,i}^{k}\mathbf{V})+\Gamma_{k,i}^{k}}}\right)$$
$$= \log_2\left(\frac{\sum_{t=i}^{M_k}(\mathrm{tr}(\mathcal{R}_{k,i}^{k}\mathbf{V})+\Gamma_{k,i}^{k})p_{k,t}+\sum_{j=1,j\neq k}^{K}(\mathrm{tr}(\mathcal{R}_{k,i}^{j}\mathbf{V})+\Gamma_{k,i}^{j})\sum_{l=1}^{M_j} p_{j,l}+\sigma^2}{\sum_{t=i+1}^{M_k}(\mathrm{tr}(\mathcal{R}_{k,i}^{k}\mathbf{V})+\Gamma_{k,i}^{k})p_{k,t}+\sum_{j=1,j\neq k}^{K}(\mathrm{tr}(\mathcal{R}_{k,i}^{j}\mathbf{V})+\Gamma_{k,i}^{j})\sum_{l=1}^{M_j} p_{j,l}+\sigma^2}\right). \quad (42)$$

convex one. By applying the first-order Taylor expansion, we have

$$\widehat{g}_{k,i}(\mathbf{V}) \leq \widehat{g}_{k,i}(\mathbf{V}^{(m)}) + \mathrm{tr}\left((\nabla_{\mathbf{V}}\widehat{g}_{k,i}(\mathbf{V}^{(m)}))^H(\mathbf{V}-\mathbf{V}^{(m)})\right) \triangleq \widehat{g}_{k,i}(\mathbf{V},\mathbf{V}^{(m)}), \quad (45)$$

$$\nabla_{\mathbf{V}}\widehat{g}_{k,i}(\mathbf{V}^{(m)}) \triangleq \frac{\sum_{t=i+1}^{M_k}(\mathcal{R}_{k,i}^{k})^H p_{k,t}+\sum_{\substack{j=1,\\ j\neq k}}^{K}\sum_{l=1}^{M_j}(\mathcal{R}_{k,i}^{j})^H p_{j,l}}{\left(\mathrm{tr}(\mathcal{R}_{k,i}^{k}\mathbf{V}^{(m)})\sum_{t=i+1}^{M_k}p_{k,t}+\sum_{\substack{j=1,\\ j\neq k}}^{K}\sum_{l=1}^{M_j}\mathrm{tr}(\mathcal{R}_{k,i}^{j}\mathbf{V}^{(m)})p_{j,l}+\overline{\beta}_{k,i}\right)\ln 2},$$

where $\widehat{g}_{k,i}(\mathbf{V}^{(m)})$ is the mth iteration of $\widehat{g}_{k,i}(\mathbf{V})$. Substituting (45) into (44b) and omitting constraint (44e), (P3.1) is rewritten as

$$(\mathrm{P3.2}): \min_{\mathbf{V}} \ P_{sum} \quad (46a)$$
$$\text{s.t. } \widehat{f}_{k,i} - \widehat{g}_{k,i}(\mathbf{V},\mathbf{V}^{(m)}) \geq R_{min}, \quad (46b)$$
$$[\mathbf{V}]_{nn} = 1, n = 1,2,\cdots,N+1, \quad (46c)$$
$$\mathbf{V} \succeq 0. \quad (46d)$$

(P3.2) is a convex optimization problem. However, the solution of (P3.2) may not satisfy the rank-one constraint. As such, a Gaussian randomization procedure is employed to yield a high-quality solution of (P3.2) [40]. First, the eigenvalue decomposition of $\mathbf{V}$ can be expressed as $\mathbf{V} = \mathbf{U}\Sigma\mathbf{U}^H$, where $\mathbf{U}$ denotes the unitary matrix and Σ represents the diagonal matrix [41]. Next, let $\Sigma^{\frac{1}{2}} \triangleq \mathrm{diag}\left\{\sqrt{\zeta_1},\sqrt{\zeta_2},\cdots,\sqrt{\zeta_{N+1}}\right\}$, we thus define $\widetilde{\mathbf{e}} = \mathbf{U}\Sigma^{\frac{1}{2}}\mathbf{S}$, where $\mathbf{S} \sim \mathcal{CN}(\mathbf{0},\mathbf{I}_{N+1})$. For any $\widetilde{\mathbf{e}}$, it holds that

$$\widetilde{\mathbf{e}}^H\widetilde{\mathbf{e}} = \mathbf{S}^H(\Sigma^{\frac{1}{2}})^H\mathbf{U}^H\mathbf{U}\Sigma^{\frac{1}{2}}\mathbf{S} = \mathrm{tr}(\Sigma\mathbf{S}\mathbf{S}^H) = \mathrm{tr}(\Sigma) = \mathrm{tr}(\mathbf{V}^*). \quad (47)$$

Using (47), the closed-form expression of the RIS reflecting coefficients in problem (P3.2) is written as

$$\Theta^* = \mathrm{diag}\left\{e^{j\angle\frac{\widetilde{\mathbf{e}}[1]}{\widetilde{\mathbf{e}}[N+1]}}, e^{j\angle\frac{\widetilde{\mathbf{e}}[2]}{\widetilde{\mathbf{e}}[N+1]}},\cdots,e^{j\angle\frac{\widetilde{\mathbf{e}}[N]}{\widetilde{\mathbf{e}}[N+1]}}\right\}. \quad (48)$$

The RIS reflecting coefficients Θ^* are selected from the set of all feasible solutions $\{\Theta\}$ through multiple iterations that satisfies all constraints, and thus minimizes the total cost of the RIS-assisted multi-UAV system. Next, we focus on solving the transmit power $\{\mathbf{P}\}$ via the standard convex optimization methods.

C. Transmit Power Optimization

With fixed $\mathbf{q}$, Θ and $\mathbf{u}$, problem (P1) is written as

$$(\mathrm{P4}): \min_{\mathbf{P}} \ P_{sum} \quad (49a)$$
$$\text{s.t. } p_{k,i} \geq 0, \quad (49b)$$
$$\log_2(1+SINR_{k,i}) \geq R_{min}. \quad (49c)$$

(P4) is non-convex due to constraint (49c). To overcome this issue, we transform the constraint (49c) via logarithmic transformations as

$$\omega_{k,i}^{k}p_{k,i} + (1-2^{R_{min}})\left(\omega_{k,i}^{k}\sum_{t=i+1}^{M_k} p_{k,t} + \sum_{j=1,j\neq k}^{K}\omega_{k,i}^{j}\sum_{l=1}^{M_j} p_{j,l}\right) + \sigma^2 \geq 0. \quad (50)$$

By substituting (50) into problem (P4), it can be equivalently expressed as

$$(\mathrm{P4.1}): \min_{\mathbf{P}} \ P_{sum} \quad (51a)$$
$$\text{s.t. } p_{k,i} \geq 0, \quad (51b)$$
$$(50) \quad (51c)$$

Problem (P4.1) is a convex optimization problem, and thus can be tackled by standard convex optimization methods [37].

D. User Ordering for NOMA

Note that the solutions of the above-mentioned subproblems are obtained for a given decoding order $\mathbf{u}$. In this subsection, we will investigate a NOMA-based decoding order scheme to further enhance the system performance. One suitable approach is to apply the Brute-Force search method to find the optimal decoding order, but the computational complexity of this solution is $\mathcal{O}(K!)$. Thus, this approach is not practical due to its high computational complexity. From (12g), it can be observed that the NOMA decoding order depends on the cascaded channel gains over all users [42]. Motivated by this, we propose a dynamic-order decoding strategy to obtain $\mathbf{u}$ by considering the effect of UAV's placement, RIS reflection coefficients and transmit beamforming vectors. In the case where the combined channels between users are different, we have

$$u_k(i) > u_k(t), \text{if } \left\|\mathbf{h}_{k,i}^{k}+\mathbf{r}_{k,i}^{H}\Theta\mathbf{g}_k\right\|^2 > \left\|\mathbf{h}_{k,t}^{k}+\mathbf{r}_{k,t}^{H}\Theta\mathbf{g}_k\right\|^2, \forall i,t \in M_k. \quad (52)$$

From (52), the users with weak channel conditions are decoded first which guarantees the fairness among the users served by the same resource block. In the case of multiple users with the same combined channel gain, i.e., $\left\|\mathbf{h}_{k,i}^{k}+\mathbf{r}_{k,i}^{H}\Theta\mathbf{g}_k\right\|^2 = \left\|\mathbf{h}_{k,t}^{k}+\mathbf{r}_{k,t}^{H}\Theta\mathbf{g}_k\right\|^2, \forall i,t \in M_k$, the decoding order depends on the distance between RIS and users that is given by

$$u_k(i) < u_k(t), \text{if } \| \mathbf{w}_r - \mathbf{w}_t^k \|^2 \leq \| \mathbf{w}_r - \mathbf{w}_i^k \|^2, \forall i,t \in M_k. \quad (53)$$

TABLE I: THE JOINT UAV DEPLOYMENT AND RESOURCE ALLOCATION ALGORITHM

1: Initialize $\left(\mathbf{q}^{(m)}, \Theta^{(m)}, \mathbf{P}^{(m)}, \mathbf{u}^{(m)}\right)$;
Iterate index: m=1;
2: **ITERATE**
$\trianglerighteq$ For given $\Theta^{(m)}$, $\mathbf{P}^{(m)}$, $\mathbf{u}^{(m)}$, solve (P2.2) by CVX, then calculate $\mathbf{q}^{(m)}$ and $\mathbf{x}^{(m)}$;
$\trianglerighteq$ For given $\mathbf{q}^{(m)}$, $\mathbf{P}^{(m)}$, $\mathbf{u}^{(m)}$, obtain $\mathbf{V}^{(m)}$ via solving (P3.2), then calculate $\Theta^{(m)}$ by the Gaussian randomization procedure;
$\trianglerighteq$ For given $\mathbf{q}^{(m)}$, $\Theta^{(m)}$, $\mathbf{u}^{(m)}$, solve (P4.1) by CVX, then calculate $\mathbf{P}^{(m)}$;
$\trianglerighteq$ Obtain $\mathbf{u}^{(m)}$ using dynamic-order decoding strategy;
$\trianglerighteq$ Set $m \leftarrow m+1$;
3: **UNTIL:** Reach a predetermined number;
4: **OUTPUT:**
$\mathbf{q}^* = \mathbf{q}^{(m)}, \Theta^* = \Theta^{(m)}, \mathbf{P}^* = \mathbf{P}^{(m)}, \mathbf{u}^* = \mathbf{u}^{(m)}$.

The physical meaning of (53) is that the users farther away from the RIS can decode first, and hence the performance gain of the far users can be improved.

The overall algorithm for solving (P1) is outlined in TABLE I. In each step, (36a) is minimized over $(\mathbf{q}, \mathbf{x})$, while keeping the value of $(\Theta, \mathbf{P}, \mathbf{u})$ fixed. For a given $(\mathbf{q}, \mathbf{P}, \mathbf{u})$, Θ^* is obtained via the Gaussian randomization procedure. For a given $(\mathbf{q}, \Theta, \mathbf{u})$, $\mathbf{P}^*$ is achieved by the standard convex optimization techniques [37]. In addition, the decoding order $\mathbf{u}^*$ is optimized via the dynamic-order decoding strategy. Since (37a) is non-increasing with each iteration, our approach can converge to a fixed value which will stop if the number of iterations reach a predetermined number. The computational complexity of overall algorithm is dominated by solving four subproblems: UAV trajectory subproblem (P2.2), phase-shift matrix optimization subproblem (P3.2), transmit power optimization subproblem (P4.1) and user ordering optimization. In particular, the computational complexity of UAV trajectory subproblem is $\mathcal{O}(N_{UAV}^{3.5})$, where N_{UAV} is the number of variables in (P2.2). Since the phase-shift matrix optimization subproblem is solved by the semidefinite program (SDP) technique, its computational complexity is $\mathcal{O}((N+1)^{4.5})$ [37]. Similarly, the computational complexity of transmit power optimization subproblem is $\mathcal{O}((K)^{3.5})$. The user decoding order is determined by the NOMA-based decoding order scheme, and its computational complexity is $\mathcal{O}(1)$. In conclusion, the computational complexity of the joint UAV deployment and resource allocation algorithm is $\mathcal{O}(I_{iter}(N_{UAV}^{3.5} + (N+1)^{4.5} + K)^{3.5} + 1))$, where I_{iter} is the number of iteration for the algorithm.

IV. Numerical Results

We present numerical results to verify the performance of our designed joint UAV deployment and resource allocation algorithm. For convenience, it is assumed that the RIS-assisted multi-UAV system with $K = 2$ user groups performed by two UAVs, where each group comprises 4 users that are randomly located in a 250×250 m^2 area. It is assumed that the RIS is distributed in $(0, 250, 20)$. The specific parameters for the proposed algorithm are similar to [7], [18], [26], [36], [43], which are described in TABLE II. Note that these parameter settings are used to present the performance as an example and can be adjusted to other values relying on the considered scenarios.

TABLE II: PARAMETERS SETTINGS

Parameters	Notation	Values
The number of antennas at UAVs	N_t	32
The channel power gain	ρ_0	-30 dB
The path loss exponent	α_{ug}, α_{rg}	2.2
The Rician factor	κ_{ug}, κ_{rg}	10 dB
The altitude of UAVs	H	100m
The number of RIS reflecting elements	N	100
The noise power	σ^2	-80 dBm
The UAV power consumption	P_{UAV}	10 dBm
The power consumption of an reflecting element	P_e	0.01 dBm
The minimum inter-UAV distance	Δ_{min}	100 m
The accuracy threshold	ε_{max}	0.1

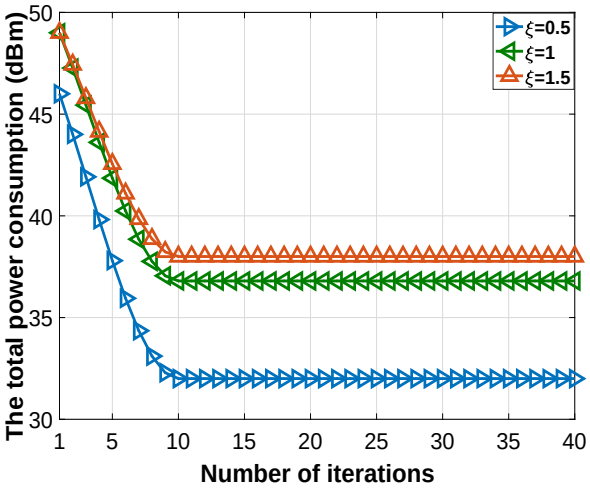

Fig. 2: An example of the convergence behavior of the joint UAV deployment and resource allocation algorithm in a RIS-assisted multi-UAV system with NOMA.

First, we investigate the convergence behavior of the joint UAV deployment and resource allocation scheme for solving the power minimization problem (P1). It is assumed that the minimum SINR value ξ is set to 0.5, 1 and 1.5 respectively. In addition, the starting points are initiated randomly in the proposed algorithm. The convergence behavior of this algorithm is examined through depicting how the total power consumption behaves with the number of iteration. As observed in Fig. 2, our proposed method with $\xi = \{0.5, 1, 1.5\}$ converges to stable values after around 10 iterations. The converged power consumption for three cases are observed to be 32, 36.5 and 38 dBm, respectively. In general, the convergence speed of the proposed algorithm depends on the joint optimization of UAV's placement, RIS reflection coefficients, power allocation and decoding order, which is the number of variables to be searched.

Next, we show the total power consumption of the

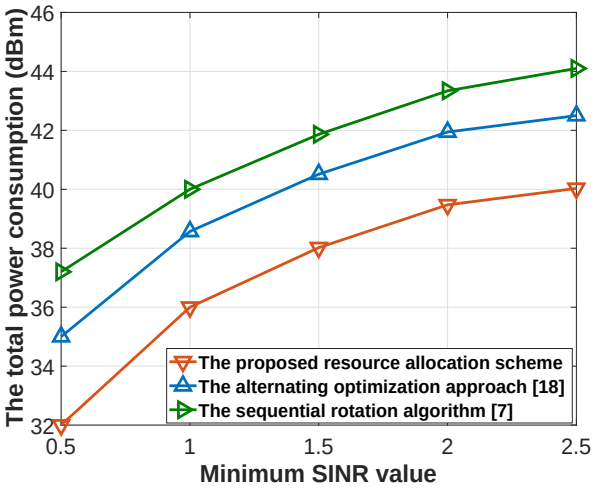

Fig. 3: The total power consumption versus the minimum SINR value under different resource allocation schemes.

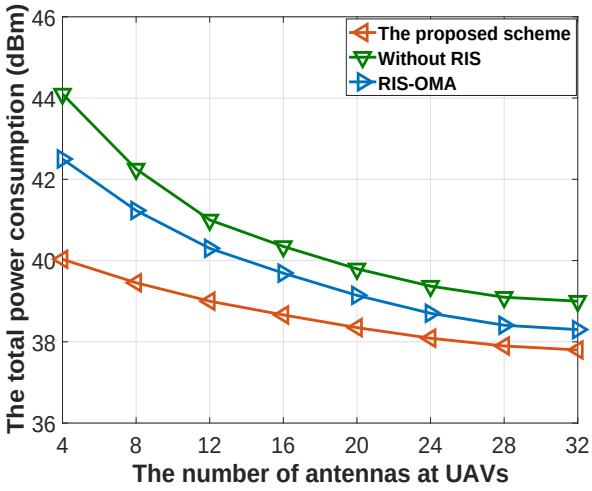

Fig. 4: The total power consumption versus the number of antennas at UAVs under different resource allocation schemes.

joint UAV deployment and resource allocation algorithm under different minimum SINR values, and compare it to the "sequential rotation algorithm" in [7] and the "alternating optimization approach" in [18]. The number of user groups is fixed to $K = 2$, while the minimum SINR value ξ varies from 0.5 to 2.5 [44]. In Fig. 3, the total power consumed by all the resource allocation schemes are non-decreasing with the minimum SINR value. This can be attributed to the fact that as the minimum SINR value rises, a higher transmit power is allocated to the combined channel in order to meet the users' QoS constraints. Moveover, the proposed method achieves better performance than that of the "sequential rotation algorithm" and the "alternating optimization approach". This is because our proposed approach exploits NOMA to serve multiple users in each resource block which can obtain a higher spectral efficiency, thereby improving the system performance. In addition, our proposed approach also employs multi-UAVs which can establish communication links with edge users such that the minimum required rate for edge users are guaranteed, and thus leads to the reduction in transmit power.

We then investigate the total power consumption of the joint UAV deployment and resource allocation scheme for various number of antennas at UAVs. To show the performance gain, we compare the algorithm that minimizes the total power consumption without RIS, and the algorithm which minimizes the overall power consumption in a RIS-assisted multi-UAV system with OFDMA. The minimum SINR value ξ is set to 1.5 and the number of reflecting element N is set to 100. As it can be seen in Fig. 4, the total power consumption achieved by all the resource allocation approaches are decreasing with an increasing number of antennas at UAVs. In fact, more antennas at UAVs can achieve higher diversity gain that balances against the extra power consumed by RF-chains, and thus consume much less transmit power [45]–[47]. Furthermore, since the proposed scheme effectively exploits RIS to improve the power levels of the received signals, it consumes much lower power compared with the "Without RIS" scheme.

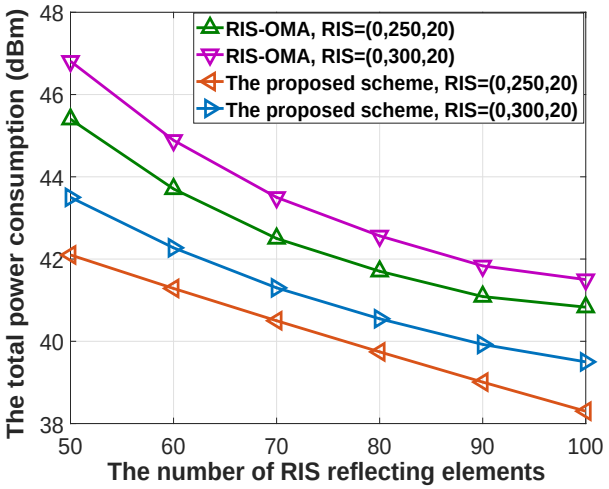

Fig. 5: The total power consumption versus the number of RIS reflecting elements under different RIS positions.

In the next simulation, the total power consumption for the joint UAV deployment and resource allocation scheme under different number of RIS reflecting units is investigated. We assume that the minimum SINR value and the number of antennas are set to $\zeta = 1.5$ and $N_t = 32$, respectively. As shown in Fig. 5, the total power consumption of all the resource allocation approaches decreases with the number of RIS reflecting elements. This is because a larger number of RIS reflecting elements can enhance the passive beamforming gain through our proposed RIS's phase-shift control, and thus leads to lower aggregation power consumption. Furthermore, it can also be seen that the placement of the RIS lies closer to the UAVs can yield a significant performance gain, which indicates that the position of the RIS can be properly selected in order to enhance the passive beamforming gain.

Fig. 6 shows the total power consumption versus the UAV's flight altitude H for different resource allocation approaches. The "RIS-OMA" and the "Without RIS" are also shown for

This article has been accepted for publication in IEEE Transactions on Communications. This is the author's version which has not been fully edited and content may change prior to final publication. Citation information: DOI 10.1109/TCOMM.2023.3298984

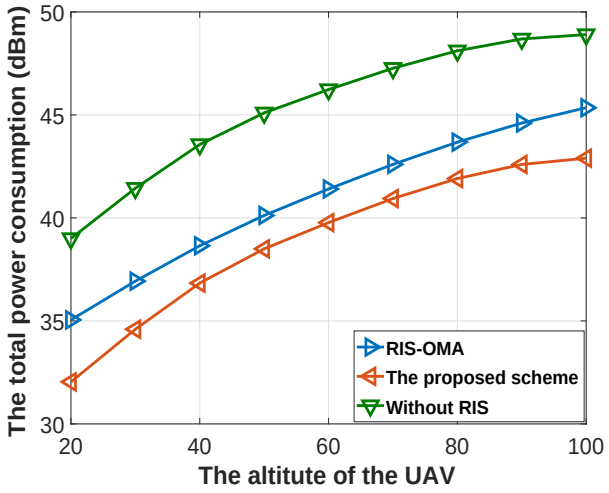

Fig. 6: The total power consumption versus the altitude of the UAV under different resource allocation schemes.

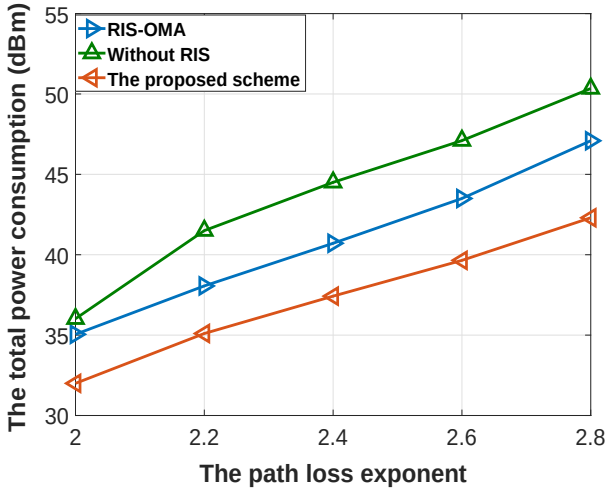

Fig. 7: The total power consumption versus the path loss exponent under different resource allocation schemes.

comparison. The SINR constraint $\zeta = 1.5$ is assumed to be equal at all users, and the UAV's height H for the proposed scheme can take value from 50m to 100m. It can be obviously observed in Fig. 6 that as H increases, the total power consumption by all the resource allocation schemes increases. In fact, UAVs hovering at higher altitude will cause severe channel attenuation and poor-signal reception. In this case, more power is allocated to UAVs for performing more effective beamforming to improve the system performance. Moreover, it can also be seen that the proposed approach provides significant power savings compared to the "RIS-OMA" and the "Without RIS" which is similar to the simulation results in Fig. 4.

Fig. 7 compares the total power consumption of all resource allocation algorithms with different values of path loss exponent. It is observed that the sum of power consumed by all the resource allocation schemes are monotonically non-decreasing with the path loss exponents. Particularly, all the schemes perform well when the path loss exponent $\alpha_{ug} = \alpha_{rg} = 2$.

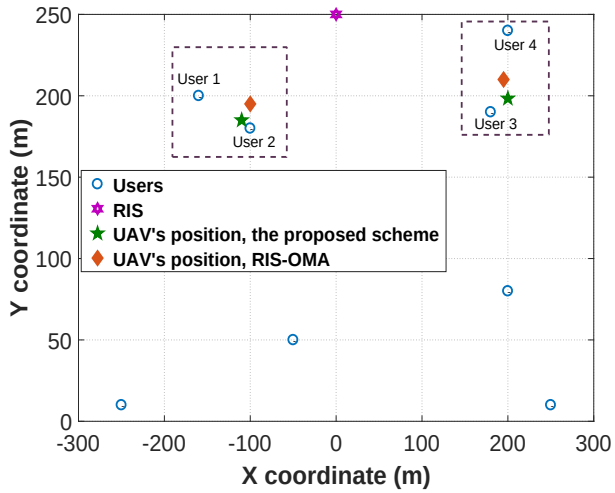

Fig. 8: The UAV deployment for a RIS-assisted multi-UAV system with NOMA.

However, the total power consumption of all the methods increases significantly thereafter, especially for the "Without RIS". The reason is that as the path loss exponents increase, the signal strength of UAV-user links and RIS-user links decreases, and thereby a higher transmit power are allocated to ensure the minimum data rate requirements of users. In addition, although a large value of α_{ug}, α_{rg} degrades the system performance, the proposed scheme still outperforms the "RIS-OMA" and the "Without RIS".

Finally, we investigate the performance of UAV deployment optimization on a horizontal plane for a RIS-assisted multi-UAV system with NOMA. The location of the RIS is fixed to $(0, 250, 20)$. As shown in Fig. 8, the positions of two UAVs obtained by our proposed scheme locate near User 2 and User 3, whilst the UAVs in the "RIS-OMA" scheme lie within the center of all users in the same group. In fact, the optimal deployment of UAVs in our proposed scheme is determined by the desired signal strength, inter-group interference as well as the minimum inter-UAV distance, such that the total power consumption can be minimized while ensuring the minimum SINR threshold as well as the fairness among users. Based on the previous simulation results, it is validated that the joint UAV deployment and resource allocation scheme can significantly reduce the total power consumption in a RIS-assisted multi-UAV system with NOMA compared with the benchmark schemes.

V. Conclusion

In this paper, we considered the RIS-aided multi-UAV system with NOMA, in which the transmit signals from multiple UAVs to all ground users were reflected through a RIS. Aiming to minimize the sum-power consumption of the system, we formulated a power minimization problem by jointly optimizing UAV's position, RIS reflection coefficients, active beamforming vectors, transmit power and decoding vectors. To tackle this problem, we first considered the sub-solutions of UAV's placement which could be achieved through the SCA and MRT. Then, the Gaussian randomization procedure

was applied to generate the closed-form solution of phase shifts at the RIS. Subsequently, effective convex optimization techniques were employed to optimize the transmit power. Furthermore, a dynamic-order decoding scheme for NOMA was then presented. Simulation results demonstrated that the total power consumption could be significantly reduced by the proposed joint UAV deployment and resource allocation algorithm compared with the benchmark methods. Our future work will study the resource allocation schemes of more general RIS-assisted multi-UAV networks with the consideration of uniform planar arrays (UPA), multiple RISs and the velocity/3D trajectory of UAVs.

APPENDIX A
PROOF OF PROPOSITION 2

We first define $\widehat{\mathbf{h}}_{k,i}^{j} = \sqrt{\frac{\gamma_{ug}}{\|\mathbf{q}_j-\mathbf{w}_i^k\|^{\alpha_{ug}}}}\overline{\mathbf{h}}_{k,i}^{j}$, $\breve{\mathbf{h}}_{k,i}^{j} = \sqrt{\frac{\rho_0-\gamma_{ug}}{\|\mathbf{q}_j-\mathbf{w}_i^k\|^{\alpha_{ug}}}}\widetilde{\mathbf{h}}_{k,i}^{j}$, $\widehat{\mathbf{r}}_{k,i}^{H} = \sqrt{\frac{\gamma_{rg}}{\|\mathbf{w}_r-\mathbf{w}_i^k\|^{\alpha_{rg}}}}\overline{\mathbf{r}}_{k,i}^{H}$ and $\breve{\mathbf{r}}_{k,i}^{H} = \sqrt{\frac{\rho_0-\gamma_{rg}}{\|\mathbf{w}_r-\mathbf{w}_i^k\|^{\alpha_{rg}}}}\widetilde{\mathbf{r}}_{k,i}^{H}$. Then, from (4) and (5), it follows that

$$\begin{aligned}\mathbb{E}\{C_{k,i}^{j}\} &= \mathbb{E}\{\| (\widehat{\mathbf{h}}_{k,i}^{j}+\breve{\mathbf{h}}_{k,i}^{j})+(\widehat{\mathbf{r}}_{k,i}^{H}+\breve{\mathbf{r}}_{k,i}^{H})\Theta\mathbf{g}_j \|^2\}\\ &= \mathbb{E}\{\|\widehat{\mathbf{h}}_{k,i}^{j}+\widehat{\mathbf{r}}_{k,i}^{H}\Theta\mathbf{g}_j\|^2\}+\mathbb{E}\{\|\breve{\mathbf{h}}_{k,i}^{j}\|^2\}+\mathbb{E}\{\|\breve{\mathbf{r}}_{k,i}^{H}\Theta\mathbf{g}_j\|^2\}.\end{aligned} \tag{19}$$

Since $\breve{\mathbf{h}}_{k,i}^{j}$ and $\breve{\mathbf{r}}_{k,i}^{H}$ are independent random variables with zero mean, in (19) we have

$$\mathbb{E}\{\|\breve{\mathbf{h}}_{k,i}^{j}\|^2\}=\mathbb{E}\left\{\left\|\sqrt{\frac{\rho_0-\gamma_{ug}}{\|\mathbf{q}_j-\mathbf{w}_i^k\|^{\alpha_{ug}}}}\widetilde{\mathbf{h}}_{k,i}^{j}\right\|^2\right\}=\frac{(\rho_0-\gamma_{ug})N_t}{\|\mathbf{q}_j-\mathbf{w}_i^k\|^{\alpha_{ug}}}, \tag{20}$$

$$\begin{aligned}&\mathbb{E}\{\|\breve{\mathbf{r}}_{k,i}^{H}\Theta\mathbf{g}_j\|^2\}\\ &= \mathbb{E}\left\{\left\|\sqrt{\frac{\rho_0-\gamma_{rg}}{\|\mathbf{w}_r-\mathbf{w}_i^k\|^{\alpha_{rg}}}}\widetilde{\mathbf{r}}_{k,i}^{H}\Theta\sqrt{\frac{\rho_0}{\|\mathbf{q}_j-\mathbf{w}_r\|^2}}\bar{\mathbf{g}}_j^T\tilde{\mathbf{g}}_j\right\|^2\right\}\\ &= \frac{NN_t\rho_0(\rho_0-\gamma_{rg})}{\|\mathbf{w}_r-\mathbf{w}_i^k\|^{\alpha_{rg}}\|\mathbf{q}_j-\mathbf{w}_r\|^2}.\end{aligned} \tag{21}$$

Substituting $\eta_{k,i} = \frac{NN_t\rho_0(\rho_0-\gamma_{rg})}{\|\mathbf{w}_r-\mathbf{w}_i^k\|^{\alpha_{rg}}}$ into (21) and associating (19)-(21) yield $\mathbb{E}\{C_{k,i}^{j}\}$ as (18). Thus, this finishes the proof of Proposition 2. ■

REFERENCES

[1] Y. Mao, C. You, J. Zhang, K. Huang, and K. B. Letaief, "A survey on mobile edge computing: The communication perspective," *IEEE Commun. Surveys Tuts.*, vol. 19, no. 4, pp. 2322–2358, 4th Quart., 2017.

[2] Z. Ding, X. Lei, G. K. Karagiannidis, R. Schober, J. Yuan, and V. K. Bhargava, "A survey on non-orthogonal multiple access for 5G networks: Research challenges and future trends," *IEEE J. Sel. Areas Commun.*, vol. 35, no. 10, pp. 2181–2195, Oct. 2017.

[3] W. Feng, N. Zhao, S. Ao, J. Tang, X. Zhang, Y. Fu, D. K. C. So, and K.-K. Wong, "Joint 3D trajectory and power optimization for UAV-aided mmWave MIMO-NOMA networks," *IEEE Trans. Commun.*, vol. 69, no. 4, pp. 2346–2358, Apr. 2021.

[4] Q. Wu and R. Zhang, "Intelligent reflecting surface enhanced wireless network via joint active and passive beamforming," *IEEE Trans. Wireless Commun.*, vol. 18, no. 11, pp. 5394–5409, Nov. 2019.

[5] Q. Wu and R. Zhang, "Towards smart and reconfigurable environment: Intelligent reflecting surface aided wireless network," *IEEE Commun. Mag.*, vol. 58, no. 1, pp. 106–112, Jan. 2020.

[6] A. S. d. Sena, D. Carrillo, F. Fang, P. H. J. Nardelli, D. B. d. Costa, U. S. Dias, Z. Ding, C. B. Papadias, and W. Saad, "What role do intelligent reflecting surfaces play in multi-antenna non-orthogonal multiple access?" *IEEE Wireless Commun.*, vol. 27, no. 5, pp. 24–31, Oct. 2020.

[7] H. Wang, C. Liu, Z. Shi, Y. Fu, and R. Song, "On power minimization for IRS-aided downlink NOMA systems," *IEEE Wireless Commun. Lett.*, vol. 9, no. 11, pp. 1808–1811, Nov. 2020.

[8] M. Fu, Y. Zhou, Y. Shi, and K. B. Letaief, "Reconfigurable intelligent surface empowered downlink non-orthogonal multiple access," *IEEE Trans. Commun.*, vol. 69, no. 6, pp. 3802–3817, June 2021.

[9] J. Zuo, Y. Liu, Z. Qin, and N. Al-Dhahir, "Resource allocation in intelligent reflecting surface assisted NOMA systems," *IEEE Trans. Commun.*, vol. 68, no. 11, pp. 7170–7183, Nov. 2020.

[10] M. Zeng, X. Li, G. Li, W. Hao, and O. A. Dobre, "Sum rate maximization for IRS-assisted uplink NOMA," *IEEE Commun. Lett.*, vol. 25, no. 1, pp. 234–238, Jan. 2021.

[11] X. Mu, Y. Liu, L. Guo, J. Lin, and R. Schober, "Joint deployment and multiple access design for intelligent reflecting surface assisted networks," *IEEE Trans. Wireless Commun.*, vol. 20, no. 10, pp. 6648–6664, Oct. 2021.

[12] F. Fang, Y. Xu, Q.-V. Pham, and Z. Ding, "Energy-efficient design of IRS-NOMA networks," *IEEE Trans. Veh. Technol.*, vol. 69, no. 11, pp. 14 088–14 092, Nov. 2020.

[13] W. Feng, J. Tang, N. Zhao, X. Zhang, X. Wang, K.-K. Wong, and J. Chambers, "Hybrid beamforming design and resource allocation for UAV-aided wireless-powered mobile edge computing networks with NOMA," *IEEE J. Sel. Areas Commun.*, vol. 39, no. 11, pp. 3271–3286, Nov. 2021.

[14] S. Zhang, H. Zhang, Q. He, K. Bian, and L. Song, "Joint trajectory and power optimization for UAV relay networks," *IEEE Commun. Lett.*, vol. 22, no. 1, pp. 161–164, Jan. 2018.

[15] W. Feng, N. Zhao, S. Ao, J. Tang, X. Zhang, Y. Fu, D. K. C. So, and K.-K. Wong, "Joint 3D trajectory design and time allocation for UAV-enabled wireless power transfer networks," *IEEE Trans. Veh. Technol.*, vol. 69, no. 9, pp. 9265–9278, Sept. 2020.

[16] G. Zhang, Q. Wu, M. Cui, and R. Zhang, "Securing UAV communications via joint trajectory and power control," *IEEE Trans. Wireless Commun.*, vol. 18, no. 2, pp. 1376–1389, Feb. 2019.

[17] S. Li, B. Duo, X. Yuan, Y.-C. Liang, and M. Di Renzo, "Reconfigurable intelligent surface assisted UAV communication: Joint trajectory design and passive beamforming," *IEEE Wireless Commun. Lett.*, vol. 9, no. 5, pp. 716–720, May 2020.

[18] Z. Wei, Y. Cai, Z. Sun, D. W. K. Ng, J. Yuan, M. Zhou, and L. Sun, "Sum-rate maximization for IRS-assisted UAV OFDMA communication systems," *IEEE Trans. Wireless Commun.*, vol. 20, no. 4, pp. 2530–2550, Apr. 2021.

[19] L. Ge, P. Dong, H. Zhang, J.-B. Wang, and X. You, "Joint beamforming and trajectory optimization for intelligent reflecting surfaces-assisted UAV communications," *IEEE Access*, vol. 8, pp. 78 702–78 712, Apr. 2020.

[20] L. Yang, F. Meng, J. Zhang, M. O. Hasna, and M. D. Renzo, "On the performance of RIS-assisted dual-hop UAV communication systems," *IEEE Trans. Veh. Technol.*, vol. 69, no. 9, pp. 10 385–10 390, Sept. 2020.

[21] H. Lu, Y. Zeng, S. Jin, and R. Zhang, "Aerial intelligent reflecting surface: Joint placement and passive beamforming design with 3D beam flattening," *IEEE Trans. Wireless Commun.*, vol. 20, no. 7, pp. 4128–4143, July 2021.

[22] T. Shafique, H. Tabassum, and E. Hossain, "Optimization of wireless relaying with flexible UAV-borne reflecting surfaces," *IEEE Trans. Commun.*, vol. 69, no. 1, pp. 309–325, Jan. 2021.

[23] H. Long, M. Chen, Z. Yang, B. Wang, Z. Li, X. Yun, and M. Shikh-Bahaei, "Reflections in the sky: Joint trajectory and passive beamforming design for secure UAV networks with reconfigurable intelligent surface," [Online], Available: https://arxiv.org/abs/2005.10559.

[24] A. Khalili, E. M. Monfared, S. Zargari, M. R. Javan, N. M. Yamchi, and E. A. Jorswieck, "Resource management for transmit power minimization in UAV-assisted RIS HetNets supported by dual connectivity," *IEEE Trans. Wirel. Commun.*, vol. 21, no. 3, pp. 1806–1822, Mar. 2022.

[25] X. Liu, Y. Liu, and Y. Chen, "Machine learning empowered trajectory and passive beamforming design in UAV-RIS wireless networks," *IEEE J. Sel. Areas Commun.*, vol. 39, no. 7, pp. 2042–2055, July 2021.

[26] X. Mu, Y. Liu, L. Guo, J. Lin, and H. V. Poor, "Intelligent reflecting surface enhanced multi-UAV NOMA networks," vol. 39, no. 10, pp. 3051–3066, Oct. 2021.

[27] Y. Zeng, R. Zhang, and T. J. Lim, "Wireless communications with unmanned aerial vehicles: opportunities and challenges," *IEEE Commun. Mag.*, vol. 54, no. 5, pp. 36–42, May 2016.

[28] S. Zargari, A. Khalili, Q. Wu, M. R. Mili, and D. W. K. Ng, "Max-min fair energy-efficient beamforming design for intelligent reflecting surface-aided SWIPT systems with non-linear energy harvesting model," *IEEE Trans. Veh. Technol.*, vol. 70, no. 6, pp. 5848–5864, June 2021.

[29] B. Zheng, C. You, and R. Zhang, "Fast channel estimation for IRS-assisted OFDM," *IEEE Wireless Commun. Lett.*, vol. 10, no. 3, pp. 580–584, Mar. 2020.

[30] C. A. Balanis, *Antenna Theory: Analysis and Design*. New York, NY, USA: Wiley, 2016.

[31] Y. Cai, Z. Wei, S. Hu, D. W. K. Ng, and J. Yuan, "Resource allocation for power-efficient IRS-assisted UAV communications," in *Proc. IEEE. ICC*, 2020, pp. 1–7.

[32] W. Wang, H. Tian, W. Ni, and M. Hua, "Intelligent reflecting surface aided secure UAV communications," 2020, [Online]. Available: https://arxiv.org/abs/2011.04339.

[33] D. Xu, Y. Sun, D. W. K. Ng, and R. Schober, "Multiuser MISO UAV communications in uncertain environments with no-fly zones: Robust trajectory and resource allocation design," *IEEE Trans. Commun.*, vol. 68, no. 5, pp. 3153–3172, May 2020.

[34] A. Khalili, A. Rezaei, D. Xu, and R. Schober, "Energy-aware resource allocation and trajectory design for UAV-enabled ISAC," 2023, [Online]. Available: https://arxiv.org/pdf/2302.10124.pdf.

[35] Y. Zeng, J. Xu, and R. Zhang, "Energy minimization for wireless communication with rotary-wing UAV," *IEEE Trans. Wireless Commun.*, vol. 18, no. 4, pp. 2329–2345, Apr. 2019.

[36] Z. Mohamed and S. Aïssa, "Leveraging UAVs with intelligent reflecting surfaces for energy-efficient communications with cell-edge users," in *Proc. IEEE. ICC Workshops*, 2020, pp. 1–6.

[37] S. Boyd and L. Vandenberghe, *Convex Optimization*. Cambridge, U.K.: Cambridge Univ. Press, 2004.

[38] M. Hua, L. Yang, Q. Wu, and A. L. Swindlehurst, "3D UAV trajectory and communication design for simultaneous uplink and downlink transmission," *IEEE Trans. Commun.*, vol. 68, no. 9, pp. 5908–5923, Sept. 2020.

[39] Y. Sun, D. Xu, D. W. K. Ng, L. Dai, and R. Schober, "Optimal 3D-trajectory design and resource allocation for solar-powered UAV communication systems," *IEEE Trans. Commun.*, vol. 67, no. 6, pp. 4281–4298, Jun. 2019.

[40] Z.-Q. Luo, W.-K. Ma, A. M.-C. So, Y. Ye, and S. Zhang, "Semidefinite relaxation of quadratic optimization problems," *IEEE Signal Process. Mag.*, vol. 27, no. 3, pp. 20–34, May 2010.

[41] R. A. Horn and C. R. Johnson, *Matrix analysis*. New York: Cambridge univ. press, 2012.

[42] Z. Ding, X. Lei, G. K. Karagiannidis, R. Schober, J. Yuan, and V. K. Bhargava, "A survey on non-orthogonal multiple access for 5G networks: Research challenges and future trends," *IEEE J. Sel. Areas Commun.*, vol. 35, no. 10, pp. 2181–2195, Oct. 2017.

[43] H. El Hammouti, M. Benjillali, B. Shihada, and M.-S. Alouini, "Learn-as-you-fly: A distributed algorithm for joint 3D placement and user association in multi-UAVs networks," *IEEE Trans. Wirel. Commun.*, vol. 18, no. 12, pp. 5831–5844, Dec. 2019.

[44] Z. Yang, W. Xu, C. Huang, J. Shi, and M. Shikh-Bahaei, "Beamforming design for multiuser transmission through reconfigurable intelligent surface," *IEEE Trans. Commun.*, vol. 69, no. 1, pp. 589–601, Jan. 2021.

[45] J. Tang, D. K. C. So, A. Shojaeifard, K.-K. Wong, and J. Wen, "Joint antenna selection and spatial switching for energy efficient MIMO SWIPT system," *IEEE Trans. Wireless Commun.*, vol. 16, no. 7, pp. 4754–4769, Jul. 2017.

[46] J. Tang, J. Luo, M. Liu, D. K. C. So, E. Alsusa, G. Chen, K.-K. Wong, and J. A. Chambers, "Energy efficiency optimization for NOMA with SWIPT," *IEEE J. Sel. Topics Signal Process.*, vol. 13, no. 3, pp. 452–466, Jun. 2019.

[47] J. Huang, A. Mukherjee, and A. L. Swindlehurst, "Secure communication via an untrusted non-regenerative relay in fading channels," *IEEE Trans. Signal Process.*, vol. 61, no. 10, pp. 2536–2550, May 2013.